Icarus 211 (2011) 222–237

Contents lists available at ScienceDirect

Icarus

journal homepage: www.elsevier.com/locate/icarus

Evidence for episodic alluvial fan formation in far western Terra Tyrrhena, Mars

Rebecca M.E. Williams [a,*], A. Deanne Rogers [b], Matthew Chojnacki [c], Joseph Boyce [d], Kimberly D. Seelos [e], Craig Hardgrove [c], Frank Chuang [a]

[a] Planetary Science Institute, 1700 E. Fort Lowell, Suite 106, Tucson, AZ 85719, United States
[b] Department of Geoscience, Stony Brook University, Stony Brook, NY 11794, United States
[c] Department of Earth & Planetary Science, University of Tennessee, Knoxville, TN 37996, United States
[d] University of Hawai'i at Manoa, Hawai'i Institute of Geophysics and Planetology, Honolulu, HI 96822, United States
[e] Johns Hopkins University, Applied Physics Laboratory, 11100 Johns Hopkins Road, Laurel, MD 20723, United States

ARTICLE INFO

Article history:
Received 12 May 2010
Revised 30 September 2010
Accepted 6 October 2010
Available online 16 October 2010

Keywords:
Mars, Surface
Geological processes
Spectroscopy

ABSTRACT

A Late Noachian-aged alluvial fan complex within Harris Crater in far western Terra Tyrrhena, Mars, is comprised of two well-defined source regions and associated discrete depositional lobes. Three fan units were recognized based on common morphological characteristics, thermal properties and spectral signatures. Although the entire fan complex has been subjected to extensive erosional degradation, the preserved morphologies record episodic fan formation and indicate the type of flow processes that occurred; the bulk of the fan surface has morphology consistent with fluvial emplacement while one fan unit exhibits a rugged surface texture with boulders consistent with a debris flow. This transition from fluvial to late-stage debris flow(s) suggests a decline in available water and/or change in sediment supply. The thermal inertia values obtained for all three fan surface units (mean values ranged from 318 to 344 J m^{-2} K^{-1} $s^{-1/2}$) are typical for coarse-grained and/or well-indurated materials on Mars, but subtle variations point to important distinctions. Variations in aeolian bedform coverage as well as the density of ridges (inferred inverted channels) and boulders contribute to these subtle fan thermophysical differences and likely reflect changes in the fan depositional mechanisms and variations in post-depositional modification histories. The majority of the alluvial fan surface has a spectral signature that is broadly similar to TES "Surface Type 2" (ST2), with some important exceptions at long wavelengths. However, a unique spectral component was identified in one of the fan units (unit 3), that likely reflects lithological differences from other fan materials. This spectral attribute of unit 3 matched locations within the western catchment providing confirmation of provenance and supporting the contention that sediment supply changed over time as the fan developed. Finally, we applied simple modeling to a well preserved subsection of the fan complex to quantify the developmental history. Using the computed eastern fan volume (32 km^3), significant water, likely from precipitation, was involved in fan construction (>50 km^3) and an extensive period of fan formation occurred over millennia or longer.

1. Introduction and geologic setting

An alluvial fan is a fan-shaped accumulation of loose, water-transported material deposited where an upland drainage emerges into a low-relief basin. In arid terrestrial environments, alluvial fan development is controlled by climatic, hydrologic, tectonic and lithologic factors (e.g., Beaty, 1990; Bull, 1991; Blair and McPherson, 1994a,b; Harvey, 1990, 1997). Terrestrial alluvial fans typically develop incrementally, with sediment transport associated with short duration, high magnitude events (such as storm induced flash floods). Alluvial fan aggradation can span timescales of several hundred thousand years, as has been documented via radiometric age-dating of rock varnish on alluvial fan surfaces in Death Valley, California (e.g., Machette et al., 2008).

On Mars, alluvial fans have been identified at a range of scales, from multi-kilometer ramps in southern highland craters (Moore and Howard, 2005) to sub-kilometer fans in Mojave Crater (Williams and Malin, 2008). Other fan-shaped landforms on Mars, often associated with valley networks, have been interpreted to be associated with standing bodies of water (as summarized in Di Achille and Hynek (2010) and Fassett and Head (2008)). Interest in examining martian alluvial fans is driven by the desire to better characterize the formation mechanisms, timescales of fluvial activity and climatic conditions necessary for fan generation.

In martian highland craters from 0° to 30°S, Moore and Howard (2005) documented several dozen large (10–40 km radial length) alluvial fans within three regional clusters in the southern

* Corresponding author. Fax: +1 520 622 8060.
E-mail address: williams@psi.edu (R.M.E. Williams).

0019-1035/$ - see front matter © 2010 Elsevier Inc. All rights reserved.
doi:10.1016/j.icarus.2010.10.001

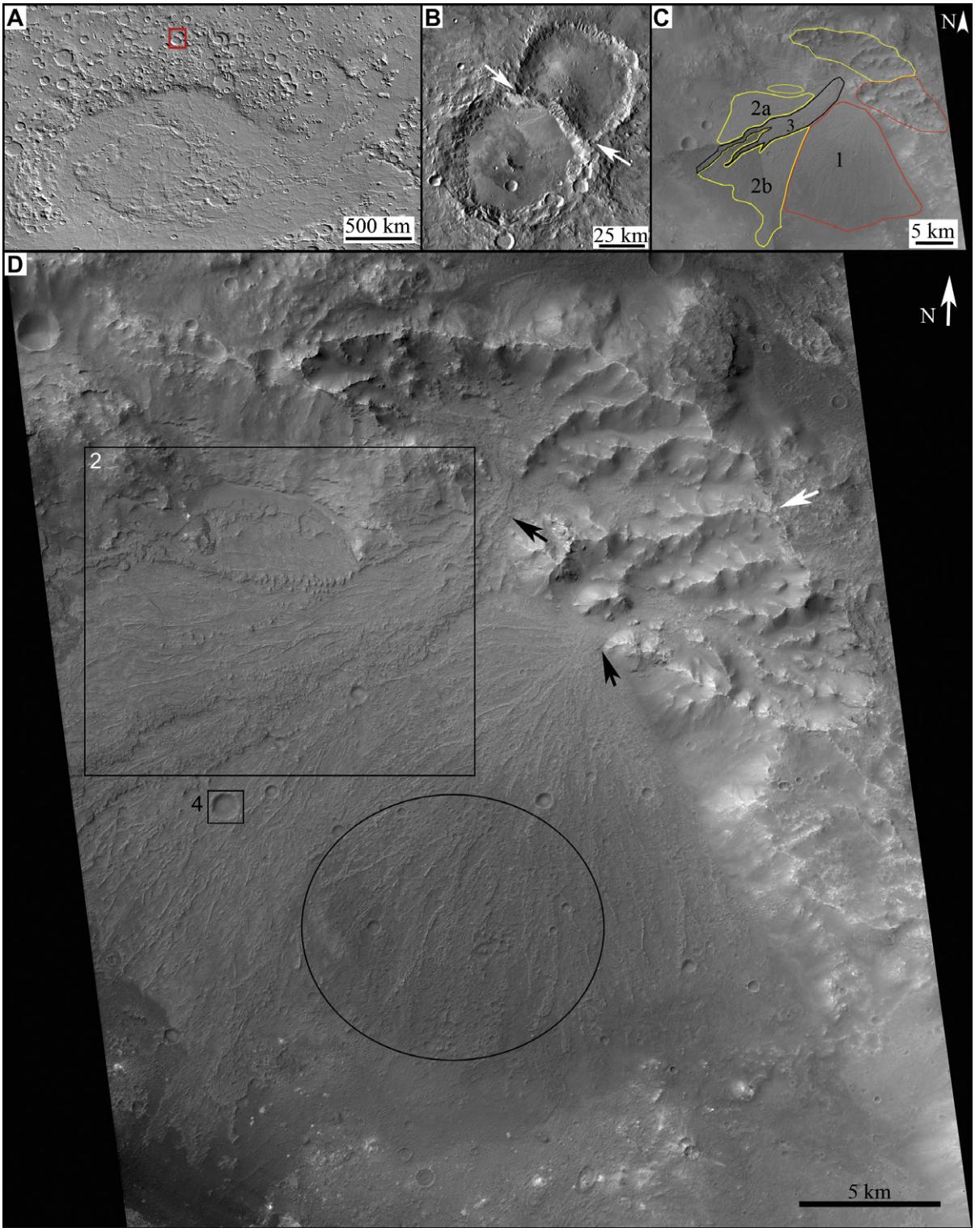

Fig. 1. (A) Regional shaded relief map of Hellas Basin with location of panel (B) identified by box. (B) Portion of THEMIS daytime infrared mosaic (Christensen et al., 2010; Gorelick and Christensen, 2005), illustrating crater setting for alluvial fan complex in this study. Two white arrows mark extent of isolated crater rim septa, the setting for the catchment basins for this alluvial fan complex. (C) Sketch map of morphological units on CTX basemap: unit 1 (eastern fan), unit 2 (western fan which has two exposures, labeled 2a and 2b) and unit 3, a swath of material originating at the mouth of the western source region and extending southwest to the crater floor atop unit 2. The eastern and western source regions are mapped with markings that correspond with the relevant fan surfaces. (D) Subscene of CTX image P14_006528_1583_XN_21S292W showing the morphology of the alluvial fan complex in Harris Crater. The two alluvial fans have distinct apexes (black arrows) and source regions, separated by ~350 m ridgeline (white arrow). Note the lighter-toned material on the eastern fan within ~5 km of the fan apex. Black oval marks darker albedo region on eastern fan, a location of abundant aeolian bedforms. Labeled boxes mark the location of subscenes illustrated in Figs. 2 and 4. Illumination is from left.

mid-latitudes. These large alluvial fans date from the Noachian–Hesperian boundary and are characterized by high-relief source areas, and a low gradient (mean slope of 2°), slightly concave longitudinal fan shape. Moore and Howard (2005) found the martian alluvial fan morphology is comparable to terrestrial alluvial fans formed via fluvial flows and infer that the era of fan formation

involved enhanced precipitation (likely snowfall). We focus on one site from that study to examine the detailed developmental history of an alluvial fan with new, high-resolution data. The study site is located on the northern rim of the Hellas Basin in Harris Crater, labeled Crater M by Moore and Howard (2005; Fig. 1).

The ~83-km diameter Harris Crater (centered at ~22.2°S, 66.9°E) superposes an earlier Noachian Crater in far western Terra Tyrrhena (Fig. 1B). Both craters exhibit evidence of degradation: the older crater to the northeast is lacking an ejecta blanket while Harris Crater has an ejecta pattern that is subdued and does not fit into the typical ejecta classification scheme of more pristine ejecta morphology as defined in Barlow's *Catalog of Large (>5 km) Martian Impact Craters* (Barlow, 1988, 2003; Barlow and Perez, 2003). The alluvial fan complex formed on the north-eastern crater rim.

2. Data and methods

In this investigation, we synthesize visible and infrared images with elevation and spectral data to unravel the geologic history of this alluvial fan complex. Medium and high-resolution visible images are from two instruments aboard the Mars Reconnaissance Orbiter (MRO): the Context Camera (CTX; Malin et al., 2007) and High Resolution Imaging Science Experiment (HiRISE, McEwen et al., 2007). The CTX acquires images up to 30 km cross-track and up to 6 m/pixel (Malin et al., 2007). HiRISE acquires images up to 6 km cross-track with a spatial resolution as high as 25 cm/pixel (McEwen et al., 2007). To date, complete CTX coverage of the alluvial fan complex has been acquired, while HiRISE images cover approximately two-thirds of the alluvial fan complex and sample all fan units. These image data were used to qualitatively assess the geomorphology of the fan complex. Area measurements were made using CTX images.

The Mars Express High Resolution Stereo Camera (HRSC; Neukum et al., 2004) level 4 digital elevation models (DEMs were used to quantitatively investigate surface morphology at 100 m/pixel (Jaumann et al., 2007; Neukum et al., 2004). Volume of the source regions was obtained through iteration. Using ARCGIS, the height for each cell (0.01 km^2) within a given region was extracted. Thus, the total volume was computed by summing the cell volumes. An estimate of fan volume, V, was made by assuming a one-quarter section of an ideal right circular cone (e.g., pie-shape wedge with sloping surface):

$$V = \frac{1}{4}\left(\frac{1}{3}\pi r^2 h\right) \quad (1)$$

where r is the radial distance and h is the height of the fan. In addition, a digital elevation model derived from a CTX stereo image pair (B10_013503_1583 and B10_013569_1584; 6 m/pixel) was used as independent confirmation of slope values and volume estimates determined from the HRSC DEM.

Thermal data is from both the Mars Global Surveyor's Thermal Emission Spectrometer (TES, 3 km/pixel between 6 and 50 μm; Christensen et al., 2001) and the Mars Odyssey's Thermal Emission Imaging System (THEMIS, 100 m/pixel, 10 bands between 6.78 and 14.88 μm; Christensen et al., 2004). Finally, the MRO Compact Reconnaissance Imaging Spectrometer for Mars (CRISM) provided spectral data with a spatial resolution of ~18 m/pixel from 0.362 to 3.92 μm with a spectral sampling of ~0.07 μm (Murchie et al., 2007).

The Mars Odyssey THEMIS instrument includes a multispectral infrared (IR) imager that measures emitted thermal infrared energy. These data may be used to characterize the thermophysical and mineralogical properties of the surface. To compute the optimal thermal inertia, the THEMIS nighttime band 9 brightness temperature is correlated with the Putzig and Mellon (2007) lookup table for the best fitting season, time of day, latitude, surface pressure, dust opacity and albedo. For materials of the same composition, thermal inertia increases with grain size, denser packing, and/or reduced pore space and therefore interpretation of thermal inertia values are not unique (e.g., Christensen, 1982, 1986; Putzig and Mellon, 2007). Higher thermal inertia values are associated with surfaces consisting of rock, duricrust, unconsolidated sand, or a mixture of these materials, while surfaces dominated by fine-grained material have a lower thermal inertia. Theoretically the effective particle size, the mean particle size of the upper few centimeters of surface material assuming that material is composed of unconsolidated homogeneous spheres, strongly influences the thermal inertia (Kieffer et al., 1973). However, when dealing with a more realistic heterogenous particle size distribution, the effective particle size is essentially equivalent to the larger particle diameters (Presley and Craddock, 2006; Presley et al., 2009). Thermal conductivity, the dominant variable in calculating thermal inertia, has been shown experimentally to be greatly influenced by the largest particle sizes in a heterogeneous particle size distribution (Presley and Craddock, 2006; Presley et al., 2009) as well as by the presence of cements (Presley et al., 2009; Piqueux and Christensen, 2009b).

Where appropriate based on meter-scale surface textures, THEMIS thermal inertia values were converted to effective particle sizes via the relationships determined by Piqueux and Christensen (2009a) for uniform spheres on non-cemented surfaces. These authors provide a model of thermal conductivity, the controlling factor in thermal inertia, which incorporates temperature in particle size derivation. This model has been validated using published laboratory measurements under a range of conditions and grain sizes.

A decorrelation stretch (DCS; Gillespie, 1992) was applied to THEMIS daytime emissivity and radiance images to visualize spectral variations in the crater and surroundings. Atmospheric components in each emissivity image were removed using the method of Bandfield et al. (2004). Average surface emissivity spectra were then selected from regions of interest in order to quantify the spectral differences between each region. As part of this analysis, comparisons are also made to two thermal infrared spectral endmembers identified in global TES observations, referred to as "Surface Type 1" (ST1) and "Surface Type 2" (ST2). ST1 surfaces, found primarily in low- and mid-latitude regions in the southern highlands, are dominated by plagioclase, pyroxene, and lesser amounts of olivine and high-silica phases (Bandfield et al., 2000b; Rogers and Christensen, 2007). "High-silica phases" refers to spectrally similar amorphous or poorly crystalline phases with Si/O > 0.35, and may include volcanic glass, amorphous silica, zeolites, clays, palagonite and/or allophane (Michalski et al., 2005; Rogers and Christensen, 2007). ST2 surfaces, whose type locality is in Acidalia Planitia, are dominated by plagioclase and high-silica phases, with lesser amounts of pyroxene (Bandfield et al., 2000b; Rogers and Christensen, 2007).

The THEMIS IR imager has a spatial resolution of 100 m/pixel, which allows for spectral distinctions across morphologic boundaries; however, the spectral resolution and wavelength range is not sufficient to derive mineral abundance estimates. To obtain quantitative compositional information, hyperspectral measurements from TES were also examined. Only TES spectra with surface temperatures >260 K, dust extinctions <0.15 and water ice extinctions <0.04 were used, following the methods of Rogers and Christensen (2007). Atmospheric components were removed using the linear deconvolution method (Smith et al., 2000). This method uses a library of emission spectra from minerals (Christensen et al., 2000), mineraloids, glasses, surface dust (Bandfield and Smith, 2003), martian atmospheric components (Bandfield, 2002; Bandfield et al., 2000a), and blackbody to obtain a linear

least-squares fit to the measured TES effective emissivity spectrum. Mineral abundances are simultaneously calculated during this process.

Visible/near-infrared spectral properties of regions of interest were obtained using the CRISM which measures reflected solar energy. CRISM data were corrected for atmospheric gases using the methods outlined by McGuire et al. (2009). In this technique, data are acquired from a spectrally uniform surface over a range of elevations to isolate the gas absorptions. Specifically, an empirical atmospheric transmission spectrum is generated by taking the ratio of the spectrum from the base of Olympus Mons to the top. This transmission spectrum is then scaled and removed from each spectrum of interest. These data are particularly sensitive to Fe- and/or OH-bearing minerals including olivine, pyroxene, sulfates and phyllosilicates. Spectral indices designed to identify these mineral groups from their diagnostic band positions and depths (Pelkey et al., 2007) were used to characterize mineralogic variability in the region. Full resolution (~18 m/pixel) targeted (FRT) CRISM images cover areas ~12 km^2; thus images are only available for a limited number of areas.

3. Observations

3.1. Morphology

Moore and Howard (2005) characterized this landform as an alluvial fan (which they named M1) and they identified a single catchment (100 km^2). However, with higher-resolution data, it is evident that this is an alluvial fan complex with distinct lobes and two fan apexes (Fig. 1D). Upslope of the fans, a ~350 m medial ridge subdivides the source region into two catchments, with the western catchment larger in size than its eastern counterpart (Fig. 1D, Table 1). The source region is characterized by steep-walled scalloped alcoves.

Table 1
Geomorphic data for alluvial fan complex on northern rim in Harris Crater.

	West	East
Catchment area (km^2)	55	40
Catchment volume (km^3)	25	20
Fan area (km^2)		
Exposed	100	165
Inferred	130	

Three fan units were initially identified based on surface morphology (Figs. 1C and 2). Unit 1, also referred to as the eastern fan, is triangular in plan form and characterized by long, narrow (<200 m), low-relief (<10 m), flat-topped radiating ridges that originate at the fan apex and traverse down slope, sometimes branching at their distal ends. Ridges superpose and cross-cut one another. Similar radiating ridges were observed on many of the fan surfaces in the Moore and Howard (2005) study, and were interpreted to be inverted channels, the remnants of a fan distributary channel system. At sub-meter-scale, layering is evident on vertical exposures of these inverted channels and records multiple flow events and few meter-sized blocks are present on the unit 1 surface (Fig. 3A). There are discrete locales where aeolian bedforms are present due to sediment trapping in topographic lows. Lighter-toned material occurs in a circular sector of the proximal fan (Fig. 1D), a region that has fewer aeolian bedforms than the dar-

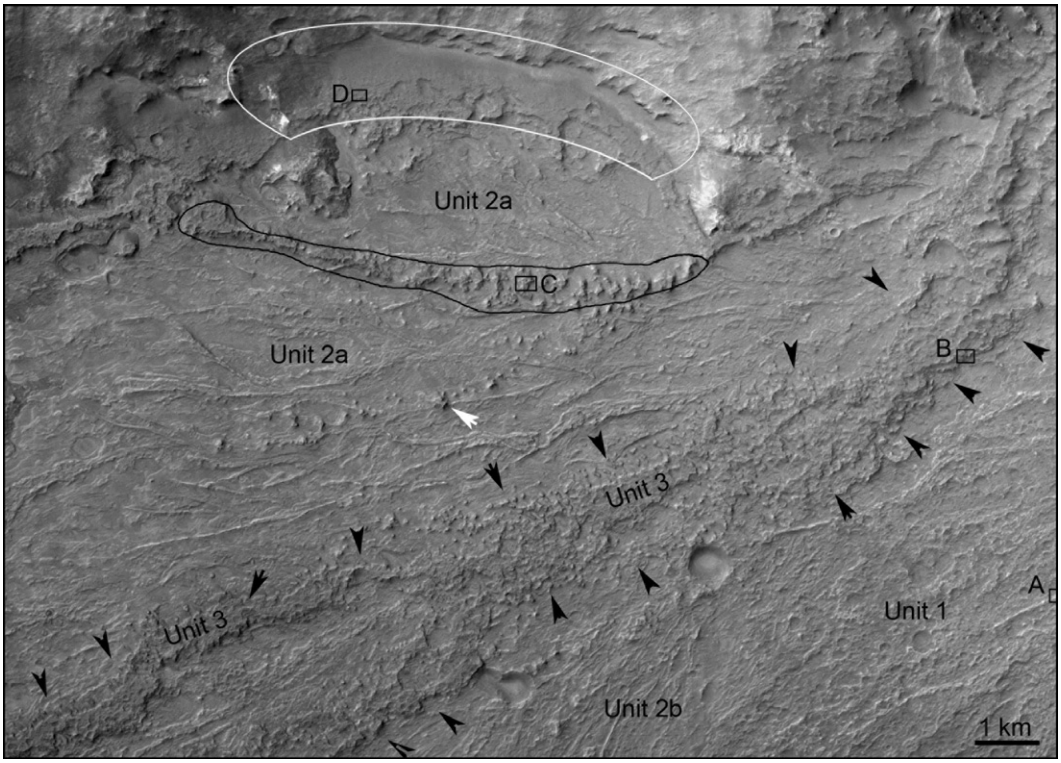

Fig. 2. This subscene of CTX image P14_006528_1583_XN_21S292W illustrates the differences in the surface textures of the fan units. Unit 1 (lower right corner) and unit 2 surfaces are characterized by linear ridges with different orientations. Some of the ridges in unit 2 are laterally traceable beneath knobs (white arrow), suggesting former burial of this surface. The unit 3 (outlined by black arrows) morphology differs from the other fan surfaces and is characterized by a rugged and pitted meter-scale surface. Larger regions of continuous unit 3 material have a flat top (e.g. location of 'Unit 3' labels). Unit 3 appears to be composed of less consolidated material, and appears to be more easily eroded relative to adjacent fan units, resulting in discontinuous patches of unit 3 as mesas and knobs. A grouping of mesas (black outline) and a ledge of material on the northwestern border of the alluvial fan complex (white outline) are two regions that have comparable spectral signatures (Fig. 7B) and may be an extension of unit 3 materials. Illumination is from the left. Lettered boxes are locations of Fig. 3.

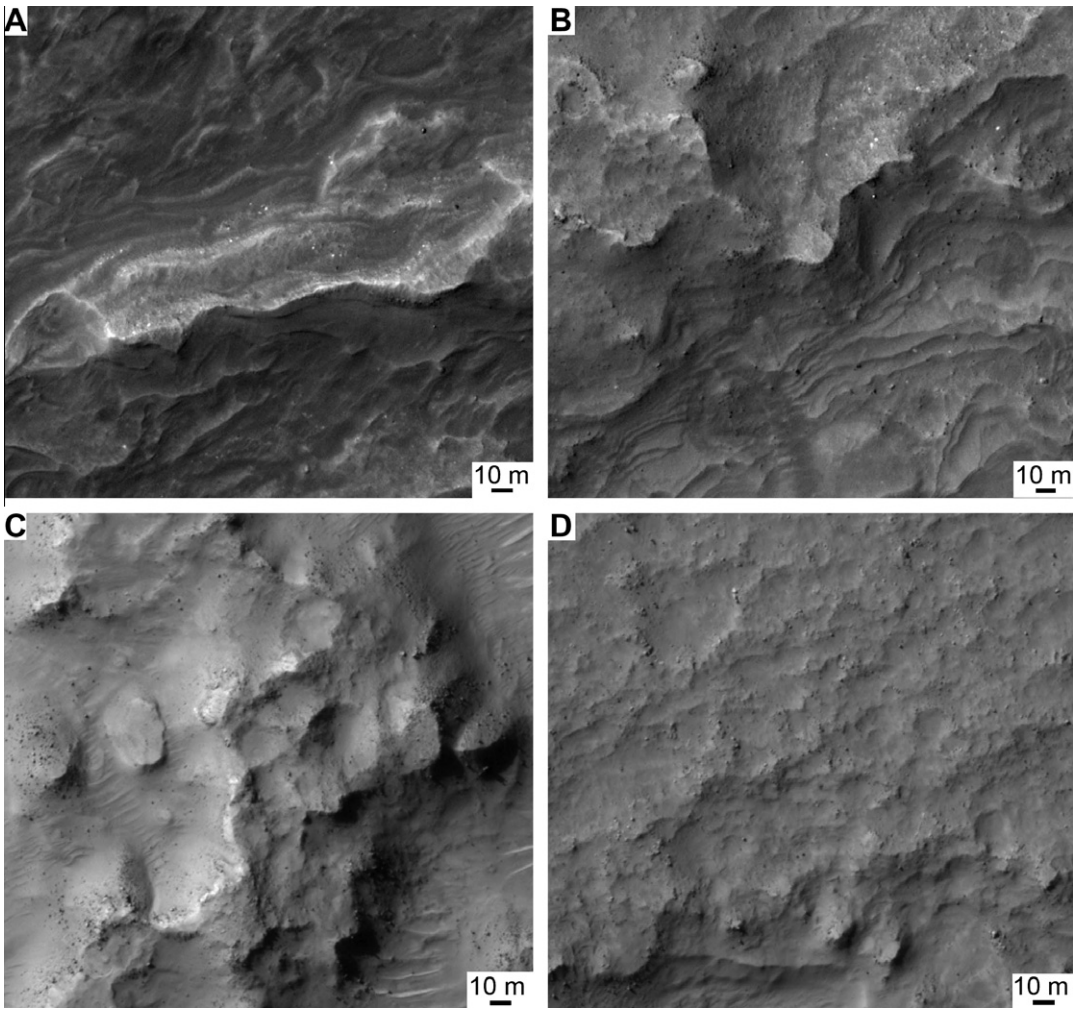

Fig. 3. High-resolution surface textures on the alluvial fan complex. Subscenes are from HiRISE images PSP_006528_1585 (panels A and B) and ESP_018738_1585 (panels C and D). See Fig. 2 for location of subscenes. Illumination is from the left. (A) Surface of eastern fan (unit 1) is characterized by linear ridges, interpreted to be inverted channels. Layering is evident in the vertical exposures of the ridges, recording multiple flow events. Very few meter-sized clasts are present on this surface. (B) The surface of unit 3 is hummocky and boulders are prevalent. A few meters beneath the bumpy and rocky top surface of unit 3, layering is present (lower-right portion of image). (C) Mesa tops are irregular surfaces similar in character at the meter-scale to unit 3. Boulders decrease in abundance with distance from the escarpment. (D) Surface of ledge northwest of the alluvial fan complex is rugged, and pitted with a high concentration of boulders, similar to the unit 3 surface.

ker-toned distal portion of the fan (Fig. 1D. The inverted ridges present in the light-toned region terminate at the transition point to the darker-toned distal fan, which suggests that these were late-stage, weaker flows that had insufficient energy to transport material across the entire fan. Impact craters on this unit are rimless and lack a discernible ejecta blanket. Layers are also evident on the crater walls (Fig. 4), a probe of the fan subsurface demonstrating multiple stages in fan aggradation. Collectively, these observations support the hypothesis that the last flow events on this fan (i.e., those exposed at the surface) were dominantly fluvial rather than debris fed. We infer that the fan surface has been subjected to aeolian erosion, which has degraded the impact craters and stripped away fines while the more erosive-resistant gravel center beds or indurated materials remain as ridges.

Unit 2, located in the western portion of the complex, is more difficult to unravel. It is subjacent to unit 3 and the eastern fan at their contact. Two low-elevation regions (Fig. 1C, regions labeled 2a and 2b) have ridges with similar attributes to those found on the eastern fan, but are locally buried by a rugged material, unit 3, that obscures their source region. In addition, there are knobs and mesas that superpose unit 2a, including a grouping of mesas that form a curvilinear path and subdivides 2a (black outline in Fig. 2); these high-standing materials are discussed in Section 4.1. Both 2a and 2b are considered to be exposures of the same fan surface, referred to as the 'western fan', and an estimate of the former contiguous surface area is given in Table 1. The northern boundary of unit 2 is marked by an arcuate ledge of material (whiteoutline in Fig. 2). Ridge orientations on unit 2 differ from unit 1 ridges (Figs. 1D and 2) and are consistent with material originating at the mouth of the western alcove. As was observed on the eastern fan, there are rimless craters superposed on the flat-topped ridge regions. Unit 2 has similar morphological attributes to unit 1, was also likely emplaced by fluvial transport processes and has been modified by aeolian erosion.

Unit 3 forms an approximately linear path from the western source region southwest to the crater floor surface, and partially buries the ridges in unit 2 by several tens of meters of rugged material. This rugged 'swath' (Fig. 1D), ranging up to 2.5 km wide, is devoid of the long, flat-topped ridges pervasive on the alluvial fan complex. Preservation of the unit is discontinuous; the unit is well preserved at the apex and subdivides into two branches downslope with other associated isolated patches (mesas and knobs). The larger patches of this unit are flat-topped. At the meter-scale, the surface is hummocky and characterized by pits,

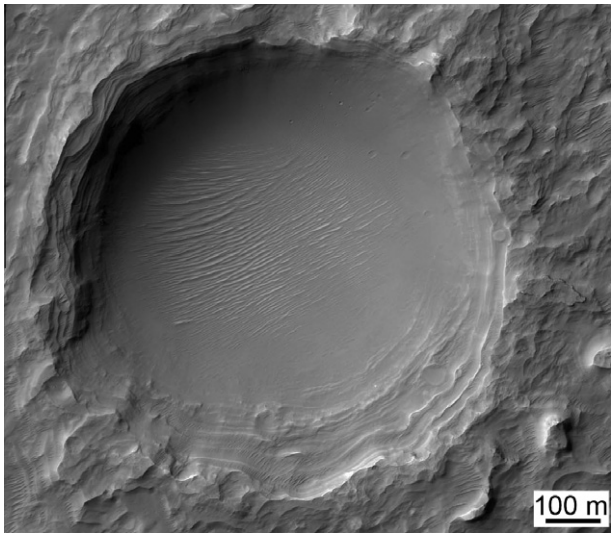

Fig. 4. Impact craters on the alluvial fan complex are rimless. Craters larger than approximately 100 m have layering on the crater walls, a record of prior flow events. The largest crater (diameter = 900 m), shown here, penetrates unit 2b. Aeolian bedforms are present on the crater floor. Figure is subscene of HiRISE image ESP_018738_1585 with illumination from the left. The location of this image is marked on Fig. 1D.

knobs and many boulders; layering is present several meters beneath the hummocky surface (Fig. 3B). Erosion of this unit has created windows to the underlying unit 2 (Fig. 2). The material deposited in unit 3 (larger coarse grain component) and the degree of induration (friable unit) contrast with the material properties observed in units 1 and 2. The morphological characteristics of unit 3 lead us to speculate that this is a heavily degraded debris flow.

Topographic data are useful in refining the relationship of fan units. The HRSC level 4 DTM is used for assessing the overall shape. However, near the resolution limit (~300 m), some inconsistencies in the data were noted; several data artifacts (>50 m rise or depressions) are present that have no obvious correlation to morphological features and craters as large as 500 m were absent in the DTM.

The eastern fan (unit 1) exhibits a classical, conical shape comparable to terrestrial alluvial fans (e.g., Blair and McPherson, 1994b) and is topographically higher than material to the west (Fig. 5). The radial profile across unit 1 is linear (Fig. 5B, Table 2), in contrast to the slightly concave up profiles observed for most of the large martian alluvial fans in the Moore and Howard (2005) study. The fan gradient derived here (2.3°) from a higher-resolution data product is slightly higher than the value (1.48°) determined by Moore and Howard (2005) from MOLA data with a resolution of 500 m/pixel. (Where exposed, the western fan (unit 2) also has a linear slope.) The eastern fan has a prominent escarpment toe (~100 m relief), which is additional evidence for modification of the fan by erosion.

Fan units can also be distinguished in transverse profiles across the alluvial fan complex. Two transverse profiles (Fig. 5C) across the alluvial fan complex illustrate that the volume of preserved fan material is larger in unit 1, which has a rounded transverse profile. Also noteworthy is the comparable elevation between unit 3 at the apex and the escarpment to the west; these two regions share similar meter-scale surface properties and spectral signatures (discussed below). We speculate that unit 3 once had a greater extent, but has largely been stripped away due to the friable nature of this material (see discussion in Section 4.1). Exposures of unit 2 are associated with the lowest elevations in the fan complex; these are inferred erosional windows into the western portion of the fan (Fig. 5C).

3.2. Age

As mapped by Greeley and Guest (1987), Harris Crater is located on terrain that is part of the Noachian plateau sequence and is characterized by subdued craters. Relative age was determined via superposition relationships, with the final flow events in each region proceeding sequentially from the western fan to the eastern fan (e.g., unit 1 surface is younger than unit 2 surface). Unit 3 postdates the final flows in the western fan (unit 2), but the timing of its emplacement relative to the later-stage eastern fan development is poorly constrained.

Crater counts are a standard technique for assessing the age of planetary surfaces. Crater counts were conducted on the fan surfaces to look for differences in crater populations (craters on unit 3 were too few to be included in this analysis; Fig. 6). Determining the age of the fan is difficult, largely due to its relatively small size. In addition, there are inherent problems in interpreting crater counts for $D < 1$ km craters (Hartmann, 2007; McEwen et al., 2005). The issue is further complicated at this site where the impact craters are clearly degraded and likely exhumed landforms. However, the crater counts suggest the fan surfaces date from the Noachian. No statistically meaningful difference in crater density was observed between the two fan surfaces; therefore any potential age difference in fan formation between the two fans is not discernible with this technique.

3.3. Thermophysical properties

Regions of comparable thermophysical properties coincide with the morphological surface units identified above. THEMIS nighttime IR images (not shown here, but patterns are consistent with the derived thermal inertia values shown in Fig. 7A) revealed the coldest surfaces associated with unit 3 and the eastern fan, whereas the western fan surface was slightly warmer. These thermal variations are not likely to be due to dust cover as this site is characterized by low to minimal TES-derived dust coverage (Ruff and Christensen, 2002).

Although the interpretation of thermal inertia values is non-unique as discussed above, when combined with morphological observations, some insight into the plausible material properties can be made. Within the study region the highest thermal inertia values (>600 J m^{-2} K^{-1} s$^{-1/2}$) were observed on crater rim spurs and the crater floor (exposed fragmented bedrock), surfaces that are presumed to be exposures of competent bedrock that is wind-swept and free of fines (Fig. 7A). The fan surfaces exhibited thermal inertia values that were slightly elevated relative to crater walls without alluvial fans. Differences in the average thermal inertia signature for the three fan units are subtle. Western fan average thermal inertia values were slightly higher (344 ± 24 J m^{-2} K^{-1} s$^{-1/2}$) than the eastern fan (318 ± 25 J m^{-2} K^{-1} s$^{-1/2}$) and unit 3 (323 ± 17 J m^{-2} K^{-1} s$^{-1/2}$) values. The occurrence of meter-size boulders do not coincide with the observed thermal inertia trends indicating that meter-size clasts are not the controlling factor in the observed thermophysical signature here. Although boulders are most abundant on the unit 3 surface, it did not have the highest mean thermal inertia value on the fan complex. The observed subtle thermal differences between fan units and within individual fans likely reflect changes in the fan depositional mechanisms and variations in post-depositional modification histories. Closer examination of the meter-scale fan surface textures is useful for understanding the thermal inertia signature.

For example, there is a longitudinal variation in thermal inertia values for unit 1, which decreases ~80 J m^{-2} K^{-1} s$^{-1/2}$ from the apex southward toward the toe. This trend is correlated with higher occurrences of aeolian bedforms in the distal portion of the fan, an area which also has a darker-toned appearance relative

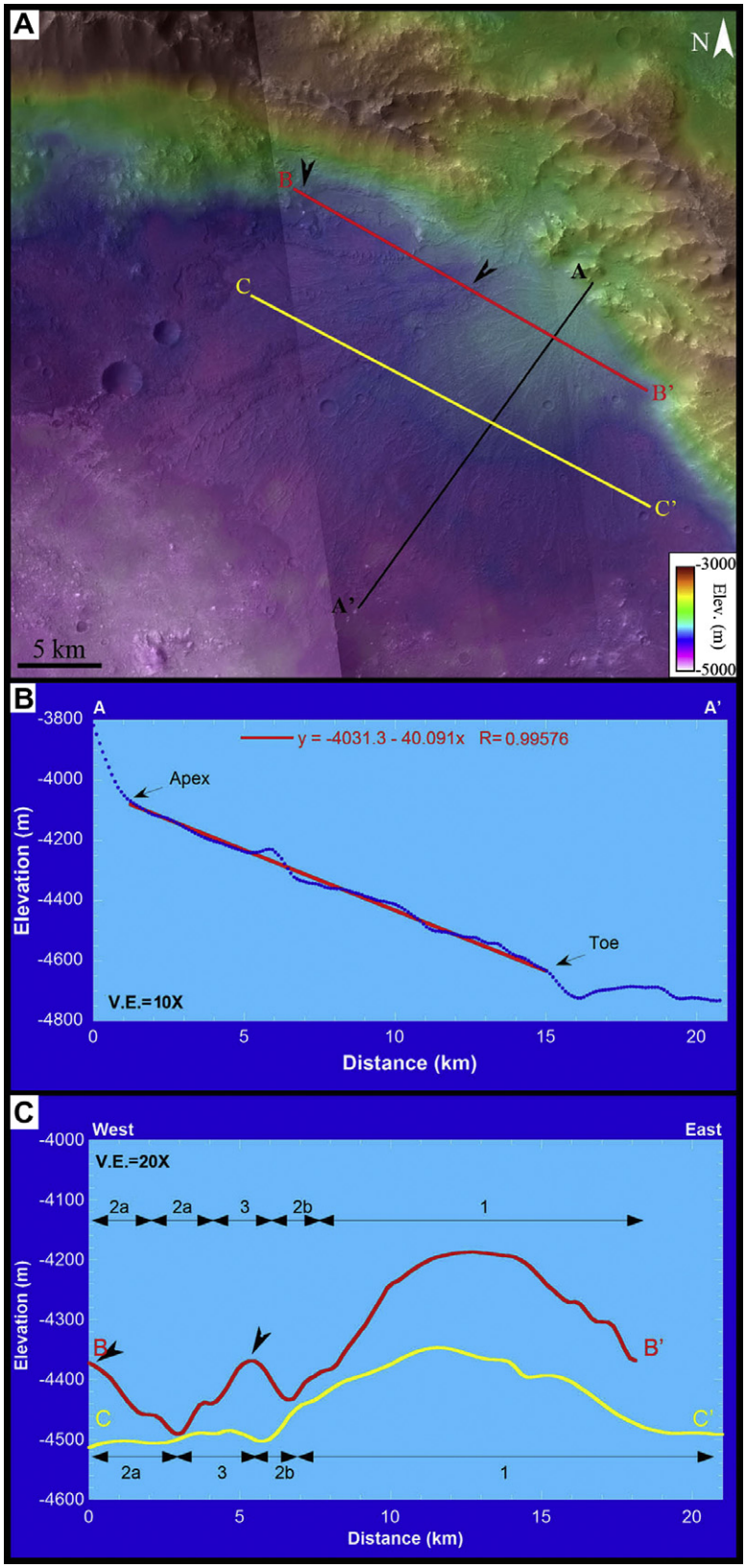

Fig. 5. (A) Digital elevation model (DEM) derived from HRSC H2549_0009 (100 m/pixel (Gwinner et al., 2008)) draped over CTX mosaic. Unit 1 has a classic conical shape and is topographically higher than material to the west. Black line A–A′ marks location of longitudinal topographic profile extracted from DEM and illustrated in (B), while color lines are transverse profiles illustrated in (C). (B) Unit 1 fan surface has a linear profile. Bump in profile near the 5 km mark is an artifact in the data, as it is present in other longitudinal profiles of the eastern fan, and has no obvious correlation to surface features. (C) Transverse profiles across alluvial fan complex, with approximate extents of different surface morphological units labeled. Unit 1 has a rounded transverse profile, consistent with its classic conical shape. In the B–B′ profile, the height of unit 3 is comparable with the ledge to the northwest (black arrows here and in panel A); these two areas also have similar spectral signatures (see Fig. 7B).

Table 2
Geomorphic data for eastern fan (unit 1).

Location	Length (km)	Relief (km)	Fan gradient (°)	Fan area (km^2)
Western fan	21.2[a]	0.52	1.6	130[b]
Eastern fan	14.7	0.57	2.3	165

[a] Approximate value as apex is buried.
[b] Due to localized burial, this is an inferred value based on regional extent and present surface exposure.

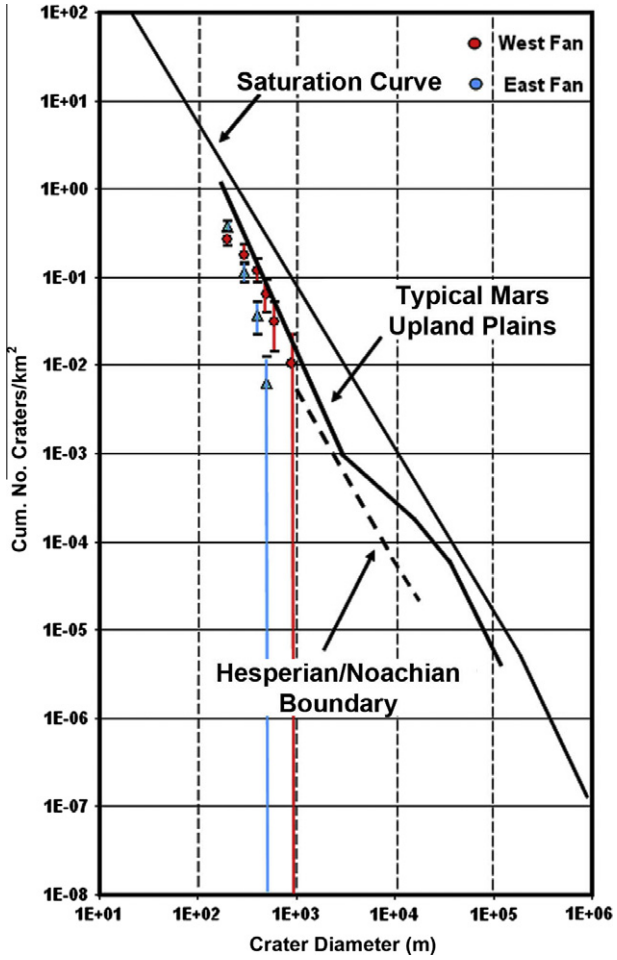

Fig. 6. Crater counts on both alluvial fan surfaces are statistically indistinguishable and consistent with a Late Noachian age. Dashed line marks the Hesperian/Noachian Boundary as defined by Tanaka (1986). Solid straight line marks the saturation curve of Hartmann (1984), and the bent solid line marks the typical Mars upland plains surface defined by Hartmann and Neukum (2001).

to other portions of the unit (Fig. 1D). Locations where bedforms have a spatial extent of several THEMIS pixels on the distal eastern fan, thermal inertia values (240–250 J m^{-2} K^{-1} s$^{-1/2}$) are consistent with 450–650 μm particle sizes or medium- to coarse-sand (Piqueux and Christensen, 2009a). Unit 1 linear ridges near the eastern fan apex (e.g., Fig. 2A) show relatively elevated thermal inertia values (370–400 J m^{-2} K^{-1} s$^{-1/2}$). The consolidated appearance of these positive relief features likely means the surface is cemented, thus raising the bulk thermal inertia (Presley et al., 2009; Piqueux and Christensen, 2009b).

As was observed on unit 1, relatively elevated thermal inertia surfaces on unit 2 are also associated with a high density of fan ridges (e.g., Fig. 2), particularly portions of northern 2a and southern 2b. Although these ridges are near the resolving limit, they often show minor elevations in thermal inertia values relative to the topographically lower adjacent areas. Unit 2 surfaces lack visible aeolian deposited material at the meter-scale and are interpreted to be more erosion-resistant portions of the fan surface where finer materials were winnowed away leaving the more consolidated fan components, as discussed above. Thus, we interpret the elevated unit 2 thermal inertia values to reflect the absence of fine-grained materials and the cementation of the fan materials.

The relatively depressed thermal inertia values and hummocky surface appearance of unit 3 suggest the material is less indurated and/or potentially friable (Fig. 2B). The relatively low thermal signature of much of unit 3 is readily distinguished from unit 2 in Fig. 7A. For example, the central portions of unit 3 (Fig. 2) have thermal inertia values of 290–340 J m^{-2} K^{-1} s$^{-1/2}$. One plausible scenario is a wide range of grain sizes, including boulders, that are weakly indurated give the erosional expression of this unit and account for the lower thermal signature of this unit relative to the well-cemented surfaces present in units 1 and 2.

Recent terrestrial analog studies of inverted paleochannels have examined the thermophysical properties of alluvial fans. The technique of using a simple temperature difference image has been found to reveal surface heterogeneities in particle size and degree of induration on fan surfaces (Hardgrove et al., 2009, 2010). In particular, for terrestrial alluvial fans in arid environments, sedimentary deposits composed of cemented material consistently were found to have higher night-time temperatures relative to the surrounding fan materials while highly friable deposits were found to have lower night-time temperatures relative to the surrounding fan materials (Hardgrove et al., 2010). Analysis of a suite of terrestrial alluvial fans supports the hypothesis that units 1 and 2 represent cemented, inverted channels while unit 3 represents more friable fan materials. While the technique used by Hardgrove et al. (2009) is not directly applicable to Mars, relative differences in night-time temperatures between fan sedimentary features on terrestrial fans provides supporting evidence for identification of martian fan sedimentary features. Future work will enable a more refined exploration of the martian datasets based on lessons learned from terrestrial analogs.

3.4. Spectral properties

The THEMIS DCS image, using bands 8 (11.8 μm), 7 (11.0 μm), and 5 (9.4 μm) displayed as red, green and blue respectively, shows spectral variability across the alluvial fan complex (Fig. 7B). However, the inverted channels in units 1 and 2 are too small to be distinguished in THEMIS, therefore their thermal infrared spectral signature is unknown. In particular, unit 3 material in this false color image appears bright yellow whereas the rest of the complex (units 1 and 2) appears pink; these regions correspond to relatively low and high thermal inertia, respectively, surfaces on the fan. THEMIS surface emissivity spectra were extracted from each of the geomorphic units within the alluvial fan complex (Fig. 8A). All three units exhibit an emissivity minimum at 9.4 μm, with an overall V-shape, similar to ST2 spectra (Bandfield et al., 2000b). Fan units 1 and 2 are spectrally indistinguishable; however, unit 3 has a slightly steeper emissivity slope between 10.2 and 12.6 μm, suggesting that it is more felsic/silicic than fan materials (Lyon, 1965). Interestingly, a comparable spectral signature to unit 3 (yellow in Fig. 7B) was observed in three locations: in the western source region, along the northwestern boundary of unit 2a in an arc of material that is topographically above the fan unit, and a group of mesas that superposes unit 2a (Figs. 2 and 7B).

Only a limited amount of quality TES data were available over the fan complex, thus only the eastern fan surface (unit 1) was sampled with TES (Fig. 8B). Unit 3 and regions with similar spectral signature in THEMIS data are too small to be resolvable in TES data.

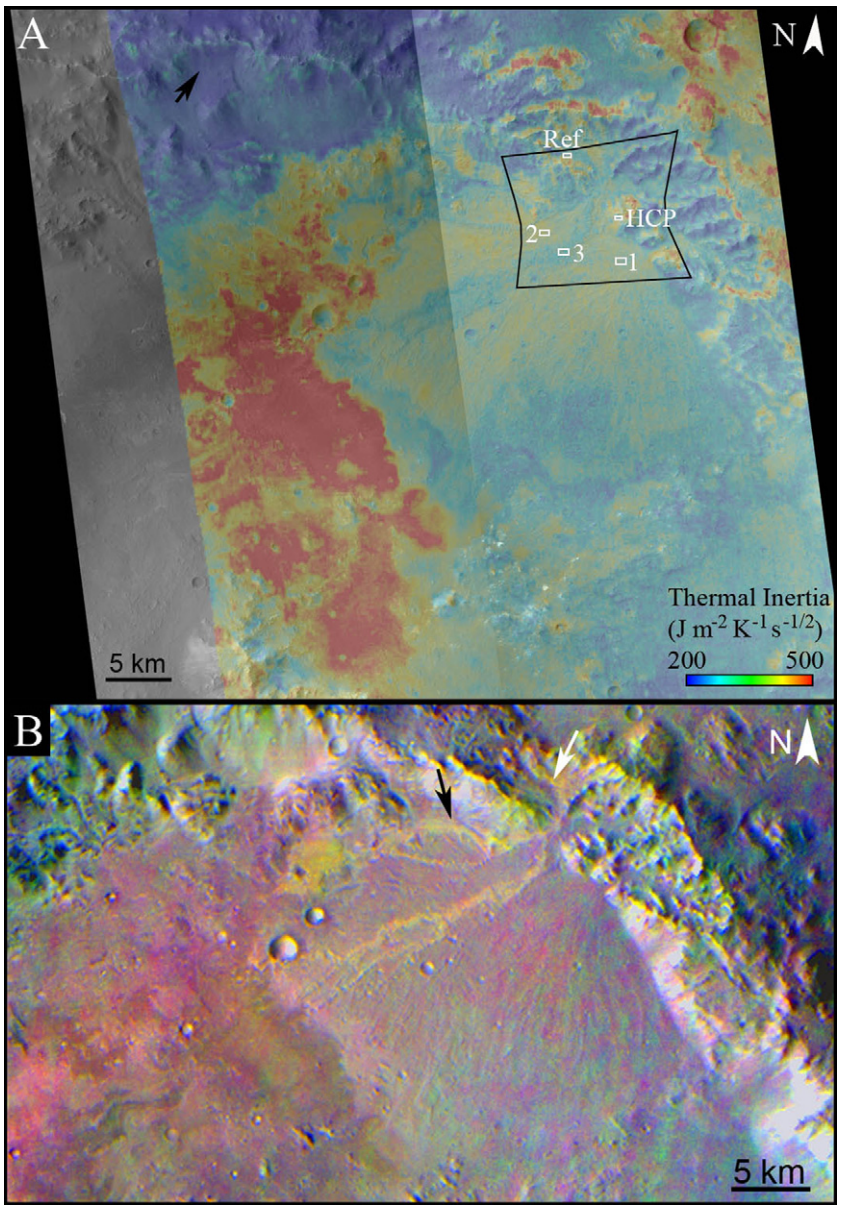

Fig. 7. (A) Thermal inertial values derived from nighttime THEMIS image I33675006 show subtle variations in thermal physical properties for the three surface units, with values consistent with coarser and/or well-indurated materials. Fan surfaces have elevated thermal inertia values relative to the crater walls without alluvial fans (example region marked by black arrow). Units 1 and 2 have similar moderate thermophysical properties, but distal portions of unit 1 shows depressed thermal inertia values, due to increased fine-grained bedform coverage. The black outline is footprint of CRISM FRT00008CF6 with spectral extraction sites indicated by white boxes (see Fig. 9). (B) A decorrelation stretch was applied to a THEMIS mosaic of daytime radiance images using bands 8–7–5 displayed as red, green and blue, respectively. A unique spectral signature is evident for unit 3, yellow here, and matches other locations in the vicinity including within the western source region (white arrow) and in an arc of material northwest of the fan (black arrow).

The model-derived mineralogical composition for the eastern fan is dominantly feldspar (30 ± 4%) and pyroxene (35 ± 4%). Lesser abundances of high-silica phases (18 + 5%) are present, and sulfates and other minerals are modeled at or below the detection limit. No olivine is detected in fan materials in the TES data. The spectral character of the fan is similar to TES ST2 between ~800–1300 cm^{-1} but dissimilar at lower wavenumbers. In particular, it lacks the strong negative slope in emissivity near 465 cm^{-1} that is indicative of high-silica phases (Ruff and Christensen, 2007), consistent with the relatively low modeled abundance of high-silica phases. A subtle shift in the band minimum between 800 and 1300 cm^{-1} towards smaller wavenumbers is also present in unit 1 relative to ST2; this is also consistent with a lack of high-silica phases relative to ST2.

One CRISM image (FRT00008CF6) covers the alluvial fan complex and source regions. Spectral index images indicate variations in olivine, pyroxene, and ferric coating within the scene (Fig. 9). Other mineral indices do not show spatially-coherent detections. On the slopes near the western fan apex is a location with elevated concentrations of high-Ca pyroxene (HCP). However, strong HCP absorptions are not apparent in unit 1 or unit 2. Though these HCP detections are mostly concentrated on Sun-facing slopes, there are also a few outcrops in the pole-facing slopes, suggesting that the detections are not false positives from viewing conditions (Pelkey et al., 2007). Also at this location, the olivine-index map suggests that there is a small outcrop of olivine-bearing materials in a separate area. However, no olivine is detected in fan materials.

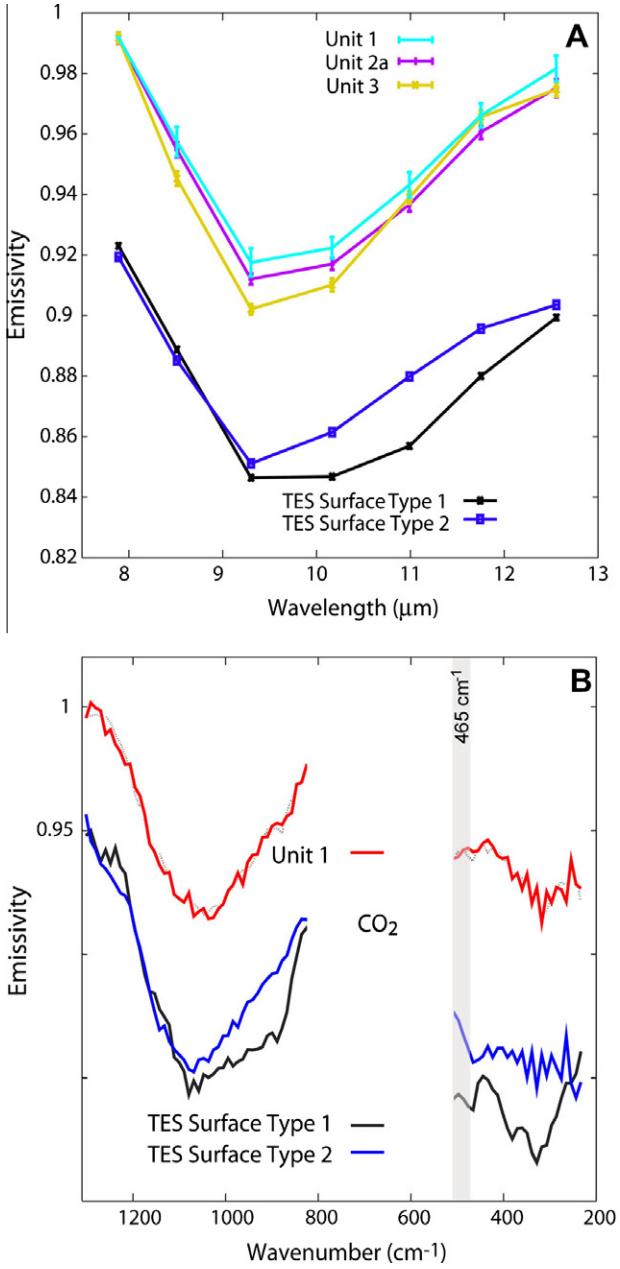

Fig. 8. (A) Average THEMIS surface emissivity spectra for the three morphologic units extracted from atmospherically-corrected THEMIS DCS image. Spectra are compared with global end-member spectra (Surface Types 1 and 2) defined from TES data. (B) TES surface emissivity spectrum and modeled surface spectrum from unit 1, compared with TES Surface Types 1 and 2. The vertical gray bar highlights the wavelength region used to calculate the 465 cm^{-1} index.

Atmospherically corrected CRISM spectra were extracted from the three morphological units, the HCP enrichment surface, the small olivine-bearing surface, and a relatively featureless reference surface (Fig. 10A). Fan surface materials are spectrally similar, with all exhibiting negative spectral slopes. These "blue" slopes are also apparent in TES ST2 regions in Acidalia Planitia, and have been attributed to ferric coatings and/or impact glass (Poulet et al., 2007) that may or may not be hydrated (Kraft et al., 2007). Negative slopes can also be caused be incomplete correction for atmospheric aerosols; however, not all surfaces in the image appear to exhibit negative slopes, suggesting that the atmospheric correction is not responsible. Pyroxene features seen by CRISM are relatively weak in the fan units. The overall spectral signature of unit 3 is also dominated by a negative spectral slope, though the slope is slightly less steep than the other fan units (Fig. 10). Average spectra from the fan units, the HCP-rich region, and the olivine-bearing surface were divided by the average spectrum from the reference surface, to enhance spectral variations between units and minimize residual atmospheric features that were not completely removed in the atmospheric correction (Fig. 10B). The spectral shapes for all fan units are similar, though they do vary slightly in overall brightness. The ratioed spectrum from the region near the western fan apex supports the HCP identification there from the summary parameter image. The "olivine-bearing" surface indicated by the olivine-index map appears to have weak hydration features and may contain smectite, or may be composed entirely of smectite. However, other than this small outcrop, there is no evidence of hydration in the alluvial fan complex or source regions.

4. Discussion

4.1. Speculation on former extent of unit 3

The alluvial fan complex has been subjected to extensive erosion, resulting in remnants of former surfaces and the exhumation of buried surfaces. Several observations suggest that unit 3 may have once been more extensive. Specifically, we examine those areas that have a comparable spectral signature to unit 3 (yellow in Fig. 7B), including an arcuate ledge of material northwest of the alluvial fan complex and a group of mesas that superposes unit 2a (Fig. 2). In addition to the similarity in spectral character, these regions exhibit comparable meter-scale surface textures: a hummocky or pitted surface with abundant boulders and a lack of layering (Fig. 3). The arcuate ledge and mesas are relatively level, consistent with the flat-topped nature of the largest portions of unit 3. These common attributes are suggestive that unit 3 once extended northwest to the crater wall and formed a continuous blanket across unit 2a. The former southeastern extent of unit 3 is less constrained as there are few mesas that superpose unit 2b. It is possible that unit 3 did extend to the southeast and portions may be buried beneath unit 1.

Interestingly, if unit 3 once covered unit 2, as we speculate, then weathering of this unit was effective in breaking down this material and there is minimal lag deposit from unit 3 present on unit 2a. In places up to 100 m of vertical relief of material was stripped to expose unit 2 (Profile B–B′ in Fig. 5C). Meter-scale boulders are relatively scarce on the unit 2 surface (e.g. Fig. 3A) and the spectral character of unit 2 is distinct from unit 3. This is consistent with a weakly consolidated material that weathers to a small particle size that could be easily transported and removed from the alluvial fan complex. These observations suggests regional variations in induration of unit 3 to explain the distribution of the preserved remnants, and is consistent with our interpretation that unit 3 is weakly indurated.

An alternative explanation is that the regions of spectral similarity to unit 3 (yellow portions of Fig. 7B) were not emplaced by unit 3 flows, but merely share a common composition (similar parent lithology or alteration product as described in next section) which explains their spectral character. These materials may preserve other alluvial flow events. In this scenario, the emplacement mechanism and timing can differ from the inferred unit 3 debris flows, but these materials were deposited between units 2 and 3.

4.2. Interpretations of spectral properties

At first glance, spectral observations presented here suggest that fan surfaces are similar to TES ST2 surfaces such as Acidalia Planitia. Thermal emission spectra from the fan are broadly similar

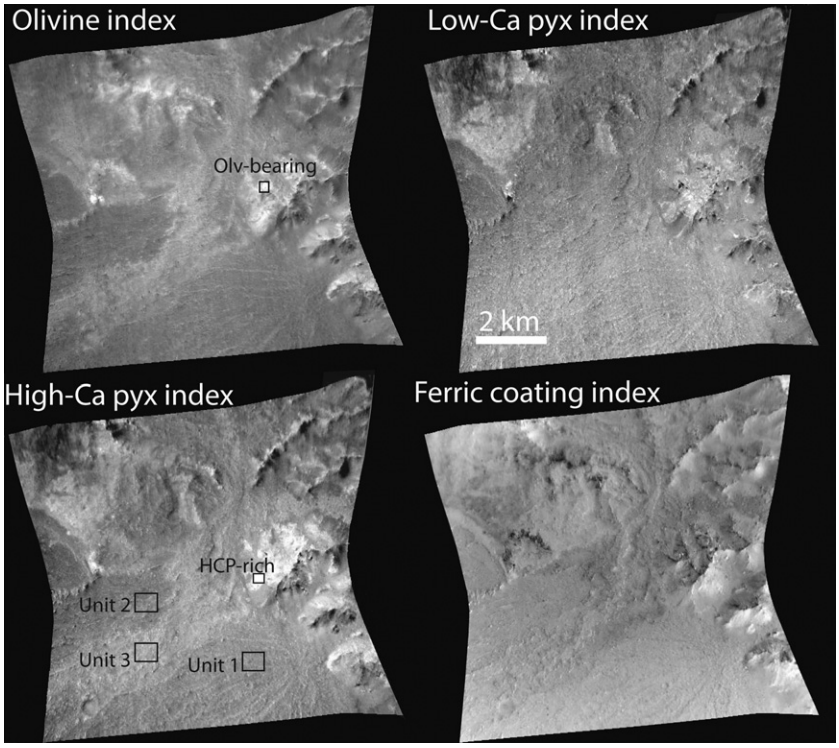

Fig. 9. Spectral index maps for CRISM. Spectral index calculations from Pelkey et al. (2007) were applied to CRISM FRT00008CF6. A standard deviation stretch was applied to each image to highlight variability in the scene.Black rectangles indicate locations of spectral averages shown in Fig. 10.

to ST2 between 800 and 1300 cm^{-1} and near-infrared spectra exhibit a strong negative slope and weak pyroxene features, consistent with ST2 (Fig. 7). However, an important difference is the lack of a negative emissivity slope at 465 cm^{-1} in fan surfaces (Fig. 7B). A strong 465 cm^{-1} feature arises from the presence of high-silica phases (Ruff and Christensen, 2007). In Acidalia, high-silica phase abundance exceeds 35% (Bandfield et al., 2000b). This observation, combined with the strong negative spectral slope in the visible/near-infrared have led to the interpretation that an amorphous silicate coating/rind containing ferric oxides (such as palagonite (Morris et al., 2003)) is the best explanation for both thermal infrared and near-infrared observations in that region (Kraft et al., 2007; Poulet et al., 2007). In the study region presented here, the lack of the 465 cm^{-1} feature over the fan units is not consistent with amorphous palagonite-like material. Rather, the negative blue slope in fan materials could be due to a ferric coating in the absence of an amorphous silicate matrix. If this is the case, the THEMIS ST2-like signature of the fan complex and swath materials might be due to olivine depletion relative to feldspar, rather than elevated high-silica phases. One might suggest that, alternatively, a ferric coating in a silicate matrix (e.g., a palagonite-like material) could be consistent with the combined observations if it is very thin (~1–2 μm); a coating of this thickness would be optically thick at short wavelengths (<12.5 μm, or <800 cm^{-1}), giving rise to the ST2-like signature in short wavelengths, but optically thin at long wavelengths (>12.5 μm), minimizing the ST2-like spectral contribution in long wavelengths. However, in controlled laboratory spectral measurements of silica-coated basalts, coatings as thin as 1 micron produce strong 465 cm^{-1} features (Kraft et al., 2003). This suggests that even a thin coating cannot explain the spectral observations presented here.

TES, THEMIS and CRISM data indicate that there is no significant mineralogical difference between the two alluvial fan complex surfaces (units 1 and 2). However both CRISM and THEMIS data indicate a subtle spectral difference between unit 3 and the fan surfaces, although these data are not easily reconciled. The spectral signature associated with the swath unit (yellow in Fig. 7B) is also found in the western source region, supporting the provenance of the unit 3 materials. CRISM data indicate that the swath material exhibits a slightly less steep negative slope, and therefore gives rise to a slightly elevated signature of pyroxene relative to fan surfaces in CRISM summary parameter images (Fig. 10). The swath material appears to have a stronger ST2-like signature in THEMIS data (Fig. 8A). If the ST2-like spectral signature of fan and swath materials were due to a thin coating (described above), one would expect the strength of the ST2 signature to increase with steepening near-infrared "blue" slope. In fact, the opposite trend is observed, further refuting the notion that the ST2-like signature is due to a palagonite-like coating. The swath material appears to have a stronger ST2-like signature in THEMIS data (Fig. 8A); unfortunately the swath material cannot be fully resolved in a TES spectrum, making it difficult to confirm the presence of increased high-silica phase abundance from the 465 cm^{-1} feature. Alternatively, a slight (~3–5%) increase in sulfate abundance in swath materials relative to fan surfaces would also be consistent with the slight differences in THEMIS signatures. If this is the case, the lack of hydration features in near-infrared data would constrain these sulfates to be anhydrous. A third explanation for the strong ST2-like signature on the swath is that it represents a more felsic lithology than the fan materials, and has less of a ferric coating. To summarize, it is clear that unit 3 is spectrally distinct from units 1 and 2, but the spectral differences could arise from a variety of scenarios. If alteration occurred, it is not clear which unit has experienced more alteration. In any case, all of these explanations imply that the spectral differences between swath and fan materials are either directly or indirectly tied to lithologic differences.

However, it is also possible that all units contained identical lithologies at the time of emplacement and that spectral distinctions could have arisen solely from weathering. The observed spectral difference between unit 3 and fan materials could reflect either

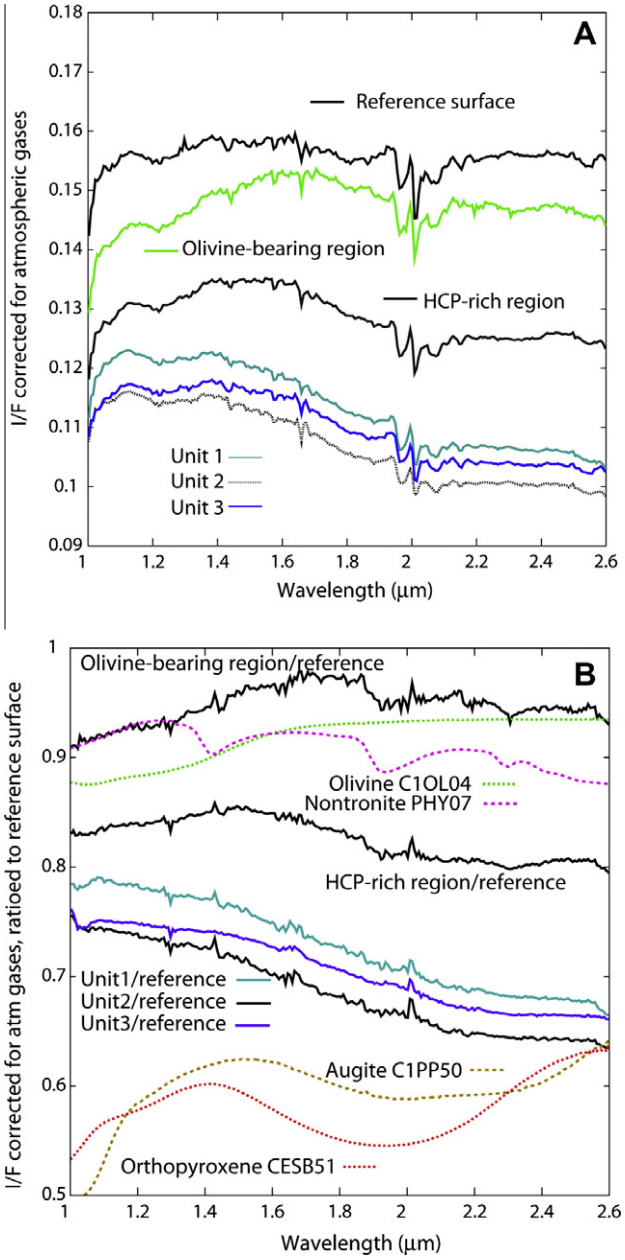

Fig. 10. (A) Atmospherically corrected CRISM I/F spectra from image FRT00008CF6. Spectra were selected from the three morphologic units as well as areas of mineral enrichment indicated from the spectral index maps (Fig. 9). A reference spectrum of a relatively featureless surface in the scene is also shown. No offsets or contrast enhancements were applied to the spectra. (B) Solid lines are spectra from A, ratioed to the reference surface. Dashed lines are spectra from the CRISM spectral library (http://http://pds-geosciences.wustl.edu/missions/mro/spectral_library.htm), shown for comparison. Library spectra were scaled and offset for more direct comparison of spectral features.

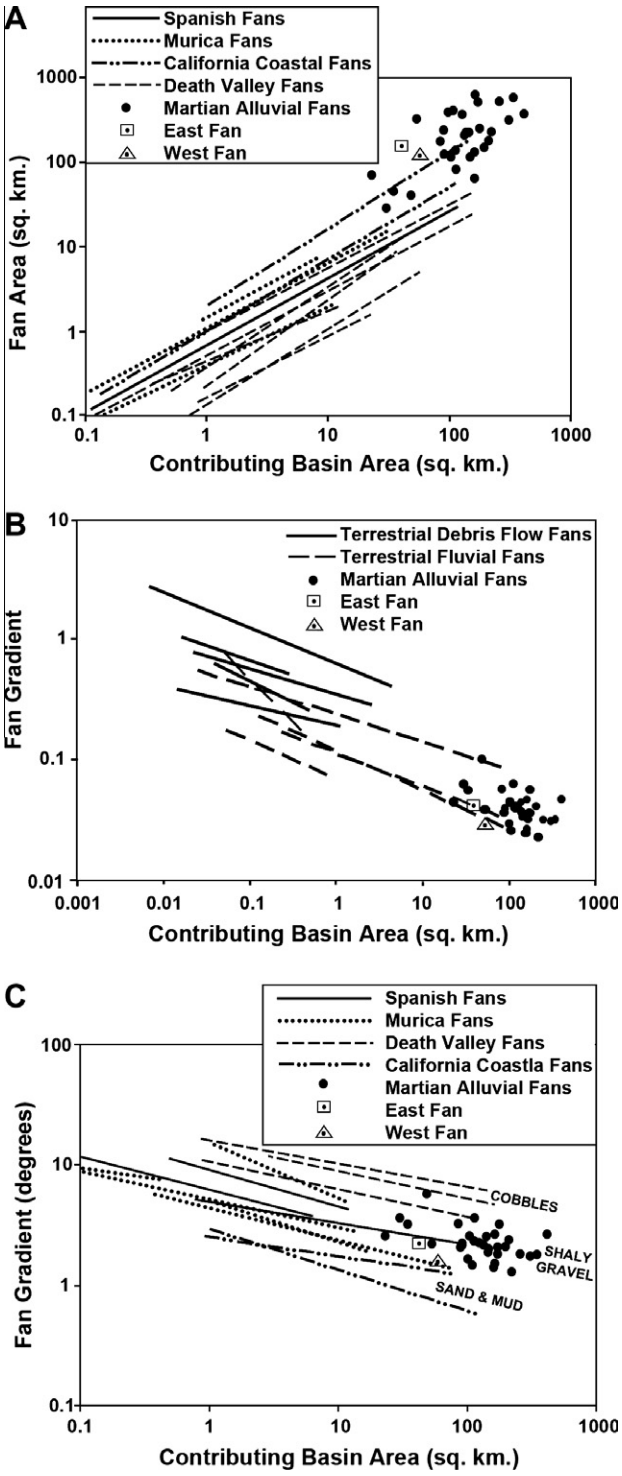

Fig. 11. Morphological plots comparing terrestrial and martian alluvial fans are modified from Moore and Howard (2005) and include terrestrial data from Harvey (1997). (A) Fan area versus contributing basin area. (B) Fan gradient versus contributing basin area. (C) Fan gradient versus contributing basin area.

(1) pre-depositional differences in alteration of identical lithologies in the source region, (2) post-depositional preferential weathering of identical lithologies, (3) differences in lithology, with relatively minimal alteration, or post-depositional preferential weathering of different lithologies. These ideas are discussed in detail below.

Pre-depositional, spatially-concentrated alteration of a lithologically uniform source region could provide the differences in mineral assemblage and thermal inertia/particle size observed between unit 3 and the other fan materials. Pre-depositional surficial weathering in the source region is not plausible, because the spectral signature and strength of unit 3 is constant from source region to distal end of unit 3. With surficial weathering, the volume of unweathered material greatly exceeds the volume of altered material. Thus during the process of erosion and deposition to form unit 3, the altered material would become mixed in with the much larger volume of unaltered material and would significantly weaken or erase any signature of pre-depositional surficial alteration. If pre-depositional alteration occurred, the explanation requires a

mechanism to concentrate alteration in a single isolated area at the surface and also at depth, such as a deep weathering front. A hydrothermal system could potentially meet these constraints, but because unit 3 is only found in a single area in the source region, we view this explanation as less likely than other scenarios involving original differences in lithology in the source region.

Post-depositional weathering of fan surfaces could also potentially give rise to the observed spectral differences between unit 3 and other fan materials. There is clear evidence of erosion producing inverted topography and exhumation of buried surfaces (e.g. unit 2a), although the relative timing of erosion is poorly constrained (e.g. the exposed unit 1 surface could pre-date or post-date emplacement of unit 3). Preferential weathering of minerals from one unit could produce a different mineral assemblage from the other depositional units, despite identical source region lithologies. Preferential weathering could be enabled by either (1) a change in weathering regime during the time that the three units were deposited, where certain units experience more weathering than younger and/or exhumed units, or (2) a difference in average particle size or particle size distribution between units, where smaller particles are more susceptible to alteration than larger ones, or (3) a difference in lithology between units, where one lithology is more susceptible to alteration than the other. Unit 3 materials are also present in the source region distinctly bounded by non-unit 3 materials, an observation that constrains the possible post-depositional alteration scenarios. The clear spatial control of unit 3 in the source region suggests that preferential alteration, if it occurred, is more likely attributed to a fundamental difference in particle size and/or lithology of unit 3 materials relative to units 1 and 2.

A third scenario is that the source regions contain multiple lithologies (igneous, sedimentary or metamorphic) which were eroded and deposited. Multiple lithologies, sampled from different depths, might be expected in crater rim materials (e.g., Fig. 2 in Shoemaker (1987)). In fact, elsewhere in southern Tyrrhena Terra region, olivine- and pyroxene-rich outcrops are abundant in crater rims (Koeppen and Hamilton, 2008) indicating that spatial variability in lithology at the scale of the unit 3 source region is plausible. A few olivine outcrops are also found in the crater rim within the study region presented here (Fig. 9). If significant alteration occurred, the differences in lithology and grain size between these units might have given rise to preferential alteration of one unit over the other under similar environmental conditions. Together these observations suggest that some unique aspect of the swath material, such as lithology, promoted stronger or weaker alteration of the swath material compared to fan surfaces. Differences in lithology also provide a robust explanation for the differences in inferred particle size between units; grain sizes produced during erosion are partly dependent on lithology (e.g., Blair, 1999). Finally, this scenario is consistent with the spectral similarity of unit 3 with regions in the western source area.

4.3. Flow processes and development timescales

Alluvial fan aggradation can occur associated with debris flows, or from either channelized or sheet flow fluvial transport. We have documented evidence for both debris flow and fluvial sedimentary deposits at the surface of a martian alluvial fan complex. The surface characteristics of unit 1, the largest fan unit, are consistent with emplacement by fluvial flows. In the western half of the complex, depositional processes transitioned from earlier fluvial (unit 2) to late-stage debris-fed (unit 3) flows that formed the swath. As debris flows have higher sediment concentration than fluvial flows, this flow regime transition reflects a decrease in fluid availability and/or increased sediment supply. Excavation of a different lithology and/or larger particle sized material in the source region is supported by the unique spectral characteristics of unit 3 relative to the other fan units, as discussed in the previous section. In addition, the differences in meter-scale surface textures in fan units support the contention that there are differences in the material properties between units 1 and 2 with unit 3.

Fan surface characteristics record later-stage events, whereas the overall fan morphology can be used to infer the nature of alluvial flow events that emplaced the volumetric bulk of the alluvial fan, specifically in terms of dominant grain size and flow type (debris flows versus fluvial transport). This approach is particularly useful in the absence of cross-sections that expose the vertical substructure of the fan where the dominant formation mechanism for the alluvial fan can be directly determined, as is done in terrestrial alluvial fan investigations. On Earth, alluvial fans are characterized by the relationship between fan gradient or area and attributes such as catchment area and sediment grain size (see reviews by Blair and McPherson (1994a) and Harvey (1997)). Applying such relationships to the martian alluvial fans is complicated due to gravity scaling uncertainties, but when these observations are combined with surface fan morphology, some inferences as to flow regime can be made.

As documented by Moore and Howard (2005), martian alluvial fans tend to have larger fan areas relative to their contributing area than their terrestrial counterpart, a relationship that holds with the revised morphometry of the eastern fan in Harris Crater presented in this study (Fig. 11A). The location of large alluvial fans within crater basins contrasts with the terrestrial mountain setting for most alluvial fans; the crater rims create a strong limitation on contributing basin size. Terrestrial debris flow-dominated fans are typically smaller and steeper (>5°) than those formed by fluvial emplacement (Blair and McPherson, 1994b). The eastern fan has characteristics consistent with fluvial formation including surface attributes (inverted channels) and topographic shape (shallow, linear fan gradient), as discussed in Section 3.1. The revised morphometric measurements determined in this study for the eastern and western fans still fall within the fluvial regime when compared to terrestrial analogs (Fig. 11B). In addition, based on such analogies, we infer the dominant grain size (volumetrically) was fairly small, likely gravel or smaller (Fig. 11C). A few larger clast-sizes (e.g., boulders) have been observed on the units 1 and 2 fan surfaces, but these may be impact ejecta or, in the case of unit 2, mass wasted material from nearby unit 3 which has a greater concentration of boulder-sized material.

Topographic data can be used to constrain the amount of water involved in fan construction. We confine our analysis to unit 1, which has a well-defined conical shape and because unit 2 is partially buried. Consistent with the planeimetric shape of unit 1, we assume the fan shape is a one-quarter section of an ideal right circular cone as described in Section 2. The intent of this exercise is to get an order of magnitude estimate of the water volume involved in forming the eastern fan. It is reasonable to ignore the underlying crater topography, which would minimally decrease the estimated fan volume (~1%). The computed fan volume from this method, is consistent with the fan volume derived from the CTX DTM, and is larger than the measured volume in the eastern source region (Table 1). Sediment bulking, a process that may be enhanced under the lower martian gravity, may partially explain why the material deposited in the fan has a larger volume than it did when it was a consolidated mass in the source region. In addition, this discrepancy may reflect material transported from the western source region, a plausible scenario given the close proximity of the two fan apexes and the unknown provenance of subsurface fan materials. However, if the eastern fan material derived exclusively from the eastern source region, then the values reported in Table 3 should be reduced by a factor of 1.6, but is still consistent with the objective of obtaining order of magnitude estimates.

Table 3
First-order estimates of water amounts necessary to construct eastern fan (unit 1).

Fan volume (km^3)	Water volume (km^3)			Water depth per unit area (km)		
	I	II	III	I	II	III
32	130	48	36	3.2	1.2	0.90

Roman numerals refer to flow regime. Assumed sediment concentration, by volume, is given in parentheses. I = fluvial flow (20%), II = hyperconcentrated flow (40%), III = debris flow (77%).

The volume of water needed is dependent on the sediment concentration in the flow. Alluvial fans constructed primarily by fluvial processes build fans incrementally by small amounts typically associated with low occurrence, high magnitude events. Sediment concentration in water flows is typically <20% by volume, but hyperconcentrated flows, 20–40% by volume, can also occur (Costa, 1988). In contrast, debris flows, a sediment-gravity process, emplace large volumes of sediment with relatively little fluid component (47–77% sediment concentration by volume) in short periods of time (Costa, 1988). For completeness, we have looked at the entire range of plausible flow regimes to estimate the associated water volume and water depth per unit area in the source region (Table 3). Minimum water volume for each flow process is estimated using the maximum sediment concentration. The flow regime for the eastern fan (unit 1) was likely dominantly fluvial, implying sediment concentrations of less than 40% by volume (simulations I and II in Table 3).

To assess the fan formation period, we consider a hypothetical scenario. Assuming a representative water release event of 5 cm with no water loss (e.g. infiltration, evaporation, etc.), estimates of the water volume necessary to construct the eastern fan equate to on the order of 10^4 events (e.g., ~64,000 purely fluvial flows). Although recurrence interval is ill-constrained, an arbitrarily assumed rate of 10 events annually, half the global annual precipitation rate on Earth (average 1 m/yr; Toon et al., 2010), equates to a development period that spans several thousand years. Thus, this rudimentary example suggests that fan formation occurred over a period of at least several millennia and more likely substantially longer.

4.4. Water source and paleoclimatic conditions

Naturally, the source of the water for these flow events is of great interest. Theoretically, groundwater or atmospheric sources are both possible. The source alcove associated with this alluvial fan complex is isolated, an attribute suggestive of a groundwater source. Indeed, the localized nature of alcove erosion on crater walls is a common attribute documented by Moore and Howard (2005) in these large-scale alluvial fans on Mars. Groundwater processes produce landforms with unique characteristics, including their morphology, planimetric pattern, and network spatial arrangement (Laity and Malin, 1985). Drainage systems that form from groundwater sapping typically develop tributaries with theater-headed alcoves that are widely spaced along a main trunk channel. Recent studies have questioned whether any terrestrial drainage system can be principally controlled by groundwater processes and the role of rapid release of water (e.g., floods) appears to be a necessary component of landscape evolution even at the classical terrestrial sapping sites (Schumm et al., 1995; Irwin et al., 2008; Lamb et al., 2006, 2007, 2008). These seepage-driven systems theoretically propagate through headward growth due to groundwater focusing and generation of new channel heads by tip-splitting as first described by Dunne (1980, 1990); this pattern markedly contrasts with the open source basin bounded steep-walled scalloped alcoves at Harris Crater. Further complicating the matter, groundwater release is typically a slow and diffuse process, one that would be unlikely to supply a sufficient discharge rate to mobilize sediment over distances of tens of kilometers to construct these alluvial fans. In addition, the location of this alluvial fan complex on an isolated crater rim makes the geometry and recharge mechanism for an aquifer difficult to envision. Specific to this site, recharge to the groundwater system would have to occur from the surrounding plateaus to the northeast and southwest along the narrow crater rim septa to the midpoint, the location of the source region, without any other expression of groundwater-fed landforms along this route (i.e., there are no seepage features or other alluvial fans associated with this portion of the impact crater basin). Finally, global-scale groundwater models for early Mars indicate that the water table deepens proximal to Hellas (Andrews-Hanna et al., 2007), which indicates that significant upwelling would be required to tap groundwater at this site.

Therefore, atmospheric precipitation is considered the more plausible water source for this site, with local topography potentially impacting the location of precipitation events. Alluvial fan formation on Earth is frequently tied to the rapid release of water, for example associated with seasonal thunderstorms or sudden snowmelt flash floods (e.g., Blair and McPherson, 1994a). These events rapidly deliver fluid to the catchment, where it is concentrated, often in the tributary network, and exits the drainage basin via the feeder channel. The source regions for Harris Crater do not have a readily identifiable drainage network, presumably due to overprinting of mass wasted material or, in the case of the western catchment, late-stage debris flows. However, the overall source region configuration, with spurs delineating narrow alcoves, is consistent with the planimetric pattern that develops from erosion via surface runoff.

It is difficult to assess the relative role of rainfall versus snowmelt in generating runoff at Harris Crater and both precipitation types were potentially involved. Snowmelt derived solely from solar radiation yields small water amounts (e.g. <mm/hr, Gray and Male, 1981); such a scenario is unlikely to contribute to most of these alluvial fan flows. Large-scale melting only occurs when there is a large amount of rain atop snow, or if there is a large and rapid increase in temperature (on the order of 10 °C over a few hours; e.g., Decaulne and Saemundsson, 2007). Certainly the late-stage debris flow that deposited unit 3 required high volumes of water either from large-scale melting or a rain event. Several lines of evidence suggest that the Noachian period had more clement climate conditions then are present today and precipitation (either as rain or snow) may have occurred (Carr and Head, 2010). Surface conditions suitable to support the surface flow of water are implied by the presence of valley networks, which are concentrated on ancient, densely cratered terrains (e.g., Mars Channel Working Group, 1983 and references therein). Morphological evidence suggests that the most intense fluvial activity in martian history was during the Late Noachian epoch (Craddock and Howard, 2002; Howard et al., 2005; Irwin et al., 2005). Higher erosion rates have been documented in the Noachian, whereas extremely low erosion rates indicate a dry and desiccating environment has prevailed since the Early Hesperian (Craddock and Maxwell,

1993; Golombek and Bridges, 2000; Golombek et al., 2006). Global mineralogical mapping suggests that Mars experienced a wet period dominated by phyllosilicate formation in the Early Noachian, followed by more arid and acidic conditions in the Late Noachina and Early Hesperian during which evaporitic sulfate deposits formed (Bibring et al., 2006). Fluvial activity during the Noachian may have only occurred only occasionally, perhaps associated with large impacts (Segura et al., 2002; Toon et al., 2010) or volcanic eruptions (Phillips et al., 2001). There remains considerable uncertainty on the forcing factors that enabled clement climate conditions to exist, the duration or periodicity of such conditions, as well as the mechanism for the transition to the current climatic regime (e.g., Carr, 1996). The results of this study demonstrate that fan formation at this location occurred over a minimum of several thousand years in the Late Noachian, although either sustained or episodic clement climate conditions are consistent with the development scenario advocated here.

5. Conclusions

The synthesis of new data reveals a multi-phase geologic history for this alluvial fan complex. Three distinct geologic deposits have been identified based on morphological, spectral and thermophysical properties: an eastern fan surface (unit 1), a western fan surface (unit 2) and a swath of rugged material (unit 3). The individual fans bulk thermal inertia mean values ranged from 318 to 338 J m^{-2} K^{-1} $s^{-1/2}$, but more detailed analysis reveal important distinctions in the fans physical properties likely related to different source materials, emplacement mechanisms and the post-depositional erosional history. The eastern and western fans (units 1 and 2) have similar moderate thermal inertia value ranges; relatively elevated local thermal properties are associated with high densities of fan ridges (inferred locations of cemented materials), whereas the distal portions of unit 1 are blanketed by aeolian bedforms which lower the thermal inertia. Unit 3 has a hummocky appearance and relatively low thermal inertia surfaces, despite the large amount of boulders; this thermal signature may reflect a range of grain sizes and/or more weakly cemented sediment in the bulk of the surface-exposed material.

The majority of the alluvial fan surface has a spectral signature that is broadly consistent with TES "Surface Type 2" (ST2), with the important exception that it lacks the strong 465 cm^{-1} feature that is characteristic of Surface Type 2 and surfaces with high abundances of high-silica phases. The spectral match between the distinct material in unit 3 and locations within the western catchment (Fig. 7B) provides independent confirmation of the provenance determined from morphological observations: the swath material originated from the western catchment. Furthermore, the meter-scale surface texture, spectral and topographic similarity between unit 3 and an arcuate deposit to the northwest suggests former lateral continuity of these materials. We conjecture that aeolian erosion has stripped away much of this younger deposit (unit 3) creating an erosional window to the older western fan deposits (units 2a and 2b).

Altogether, this study has identified discrete depositional lobes with separate source regions. The overall morphological fan characteristics are consistent with fluvial processes transporting the bulk of surface-exposed material (units 1 and 2). However, in the western portion of the alluvial fan complex there was a transition to late-stage debris flow(s), suggesting a decline in available water and/or change in sediment supply; the latter hypothesis is supported by the unique surface textures and spectral characteristics of unit 3. The proposed scenario is episodic depositional pulses over millennial timescales in the development of this alluvial fan complex, similar to typical terrestrial alluvial fan aggradation which also occurs incrementally.

Acknowledgments

We are grateful to Robert Craddock and Michael Kraft for constructive reviews of this work. Thanks are extended to David Shean (MSSS) for generating a CTX DEM. This work is supported by the National Aeronautics and Space Administration (NASA) through funding for the Mars Odyssey THEMIS science team. A.D.R. also acknowledges support from NASA MDAP NNX08AL10G. This is PSI contribution #486.

References

Andrews-Hanna, J.C., Phillips, R.J., Zuber, M., 2007. Meridiani Planum and the global hydrology of Mars. Nature 446, 163–166. doi:10.1038/nature05594.
Bandfield, J.L., 2002. Global mineral distributions on Mars. J. Geophys. Res. 107, 5042. doi:10.1029/2001JE001510.
Bandfield, J.L., Smith, M.D., 2003. Multiple emission angle surface-atmosphere separations of Thermal Emission Spectrometer data. Icarus 161, 47–65. doi:10.1016/S0019-1035(02)00025-8.
Bandfield, J.L., Christensen, P.R., Smith, M.D., 2000a. Spectral data set factor analysis and end-member recovery: Application to analysis of martian atmospheric particulates. J. Geophys. Res. 105, 9573–9587.
Bandfield, J.L., Hamilton, V.E., Christensen, P.R., 2000b. A global view of martian surface compositions from MGS-TES. Science 287, 1626–1630.
Bandfield, J.L., Rogers, D., Smith, M.D., Christensen, P.R., 2004. Atmospheric correction and surface spectral unit mapping using Thermal Emission Imaging System data. J. Geophys. Res. 109. E10008. doi:10.1029/2004JE002289.
Barlow, N.G., 1988. Crater size/frequency distributions and a revised relative martian chronology. Icarus 75, 285–305.
Barlow, N.G., 2003. Revision of the "Catalog of Large Martian Impact Craters, Sixth International Conference on Mars. Pasadena, CA (abstract #3073). <http://www.lpi.usra.edu/meetings/sixthmars2003/pdf/3073.pdf>.
Barlow, N.G., Perez, C.B., 2003. Martian impact crater ejecta morphologies as indicators of the distribution of subsurface volatiles. J. Geophys. Res. 108 (E8). doi:10.1029/2002JE002036.
Beaty, C.B., 1990. Anatomy of a White Mountain debris flow – The making of an alluvial fan. In: Rachocki, A.H., Church, M. (Eds.), Alluvial Fans – A Field Approach. Wiley, New York, pp. 69–89.
Bibring, J.P. et al., and OMEGA Team, 2006. Global mineralogical and aqueous Mars history derived from OMEGA/Mars Express data. Science 312, 400–404.
Blair, T.C., 1999. Cause of dominance by sheetflood vs. debris-flow processes on two adjoining alluvial fans, Death Valley, California. Sedimentology 46, 1015–1028.
Blair, T.C., McPherson, J.G., 1994a. Alluvial fan processes and forms. In: Abrahams, A.D., Parsons, A.J. (Eds.), Geomorphology of Desert Environments. Chapman and Hall, London, pp. 354–402.
Blair, T.C., McPherson, J.G., 1994b. Alluvial Fans and their natural distinction from rivers based on morphology, hydraulic processes, sedimentary processes and facies assemblages. J. Sediment. Res. A64 (3), 450–489.
Bull, W.B., 1991. Geomorphic Responses to Climatic Change. Oxford University Press, New York.
Carr, M.H., 1996. Water on Mars. Oxford University Press, New York. p. 229.
Carr, M.H., Head, J.W.I., 2010. Geologic history of Mars. Earth Planet. Sci. Lett. 294, 185–203.
Christensen, P.R., 1982. Martian dust mantling and surface composition: Interpretation of thermophysical properties. J. Geophys. Res. 87 (B12), 9985–9998.
Christensen, P.R., 1986. The spatial distribution of rocks on Mars. Icarus 68, 217–238.
Christensen, P.R., Bandfield, J.L., Hamilton, V.E., Howard, D.A., Lane, M.D., Piatek, J.L., Ruff, S.W., Stefanov, W.L., 2000. A thermal emission spectral library of rock-forming minerals. J. Geophys. Res. 105, 9735–9740. doi:10.1029/1998JE000624.
Christensen, P.R. et al., 2001. Mars Global Surveyor Thermal Emission Spectrometer experiment: Investigation description and surface science results. J. Geophys. Res. 106, 23823–23871. doi:10.1029/2000JE001370.
Christensen, P.R. et al., 2004. The Thermal Emission Imaging System (THEMIS) for the Mars 2001 Odyssey Mission. Space Sci. Rev. 110, 85–310.
Christensen, P.R., Gorelick, N.S., Mehall, G.L., Murray, K.C., 2010. THEMIS Public Data Releases, Planetary Data System Node, Arizona State University. <http://themis-data.asu.edu>.
Costa, J.E., 1988. Rheologic, geomorphic, and sedimentologic differentiation of water floods, hyperconcentrated flows, and debris flows. In: Baker, V.R., Kochel, R.C., Patton, P.C. (Eds.), Flood Geomorphology. John Wiley and Sons, New York, NY, pp. 439–463.
Craddock, R.A., Howard, A.D., 2002. The case for rainfall on a warm, wet early Mars. J. Geophys. Res. 107 (E11). doi:10.1029/2001JE001505.
Craddock, R.A., Maxwell, T.A., 1993. Geomorphic evolution of the martian highlands through Ancient fluvial processes. J. Geophys. Res. 98 (E2), 3453–3468.
Decaulne, A., Saemundsson, T., 2007. Spatial and temporal diversity for debris-flow meteorological control in subarctic oceanic periglacial environments in Iceland. Earth Surf. Proc. Land. 32, 1971–1983.
Di Achille, G., Hynek, B.M., 2010. Deltas and valley networks on Mars: Implications for a global hydrosphere. In: Cabrol, N.A., Grin, E.A. (Eds.), Lakes on Mars. Elsevier, pp. 223–248.

Dunne, T., 1980. Formation and controls of channel networks. Prog. Phys. Geogr. 4, 211–239.
Dunne, T., 1990. Hydrology, mechanics, and geomorphic implications of erosion by subsurface flow. In: Higgins, C.G., Coates, D.R. (Eds.), Groundwater Geomorphology: The Role of Subsurface Water in Earth-surface Processes and Landforms. Geological Society of America Special Paper, vol. 252, pp. 1–28.
Fassett, C.I., Head, J.W.I., 2008. Valley network-fed, open-basin lakes on Mars: Distribution and implications for Noachian surface and subsurface hydrology. Icarus 198, 37–56. doi:10.1016/j.icarus.2008.06.016.
Gillespie, A.R., 1992. Enhancement of multispectral thermal infrared images – Decorrelation contrast stretching. Remote Sens. Environ. 42, 147–155.
Golombek, M.P., Bridges, N.T., 2000. Erosion rates on Mars and implications for climate change – Constraints from the Pathfinder landing site. J. Geophys. Res. 105, 1841–1854.
Golombek, M.P. et al., 2006. Erosion rates at the Mars Exploration Rover landing sites and long-term climate change on Mars. J. Geophys. Res. 111 (E12). E12S10. doi:10.1029/2006JE002754.
Gorelick, N.S., Christensen, P.R., 2005. THEMIS Global Mosaics, Eos Trans. AGU 86 (52), Fall Meet. Suppl. Abstract P21C-0161.
Gray, D.M., Male, D.H., 1981. Handbook of Snow: Principles, Processes, Management, and Use. Blackburn Press.
Greeley, R., Guest, J.E., 1987. Geologic Map of the Eastern Equatorial Region of Mars. United States Geological Survey Miscellaneous Investigation I-1802-b, 1:15M Denver.
Gwinner, K., Roatsch, T., Matz, K.-D., Scholten, F., Elgner, S., Preusker, F., Oberst, J., Raumann, R., Heather, D., Neukum, G., 2008. Archival stereo data products of the HRSC experiment onboard Mars Express. Lunar Planet. Sci. Conf. LPI, Houston, TX. Abstract 2373.
Hardgrove, C., Moersch, J., Whisner, S., 2009. Thermal imaging of alluvial fans: A new technique for remote classification of sedimentary features. Earth Planet. Sci. Lett. 285, 124–130. doi:10.1016/j.epsl.2009.06.004.
Hardgrove, C., Moersch, J., Whisner, S., 2010. Thermal imaging of sedimentary features on alluvial fans. Planet. Space Sci. 58, 482–508. doi:10.1016/j.pss.2009.08.012.
Hartmann, W.K., 1984. Does crater 'saturation equilibrium' occur in the Solar System? Icarus 60, 56–74.
Hartmann, W.K., 2007. Martian cratering: 9. Toward resolution of the controversy about small craters. Icarus 189, 274–278. doi:10.1016/j.icarus.2007.02.011.
Hartmann, W.K., Neukum, G., 2001. Cratering chronology and the evolution of Mars. Space Sci. Rev. 96, 165–194.
Harvey, A.M., 1990. Factors influencing quaternary alluvial fan development. In: Rachocki, A.H., Church, M. (Eds.), Alluvial Fans – A Field Approach. Wiley, New York, pp. 109–129.
Harvey, A.M., 1997. The role of alluvial fans in arid zone fluvial systems. In: Thomas, D.S.G. (Ed.), Arid Zone Geomorphology: Process, Form and Change in Drylands. John Wiley, Hoboken, NJ, pp. 109–129.
Howard, A.D., Moore, J.M., Irwin III, R.P., 2005. An intense terminal epoch of widespread fluvial activity on early Mars: 1. Valley network incision and associated deposits. J. Geophys. Res. 110 (E12). doi:10.1029/2005JE002459.
Irwin III, R.P., Howard, A.D., Craddock, R.A., Moore, J.M., 2005. An intense terminal epoch of widespread fluvial activity on early Mars: 2. Increased runoff and paleolake development. J. Geophys. Res. 110 (E12). doi:10.1029/2005JE002460.
Irwin II, R.P., Howard, A.D., Craddock, R.A., 2008. Origin of the Theater-headed Tributaries to Escalante and Glen Canyons, Utah, Second Workshop on Mars Valley Networks, Smithsonian, Moab, Utah.
Jaumann, R., the HRSC Co-Investigator Team, et al., 2007. The High Resolution Stereo Camera (HRSC) experiment on Mars Express: Instrument aspects and experiment conduct from interplanetary cruise through nominal mission. Planet. Space Sci. 55, 928–952. doi:10.1016/j.pss.2006.12.003.
Kieffer, H.H., Chase Jr., S.C., Miner, E., Munch, G., Neugebauer, G., 1973. Preliminary report on infrared radiometric measurements from the Mariner 9 spacecraft. J. Geophys. Res. 78 (20), 4291–4312.
Koeppen, W.C., Hamilton, V.E., 2008. Global distribution, composition, and abundance of olivine on the surface of Mars from thermal infrared data. J. Geophys. Res. 113. E05001. doi:10.1029/2007JE002984.
Kraft, M.D., Michalski, J.R., Sharp, T.G., 2003. Effects of pure silica coatings on thermal emission spectra of basaltic rocks: Considerations for martian surface mineralogy. Geophys. Res. Lett. 30 (24). doi:10.1029/2003GL018848. PLA5 5-1.
Kraft, M.D., Sharp, T.G., Michalski, J.R., Rampe, E.B., 2007. Combined Thermal and Near Infrared Spectra of Hydrous Silica Coatings: Implications for Surface Type 2 Mineralogy and Recent Liquid Water on Mars. Lunar Planet. Sci. Conf. XXXVIII. Lunar and Planetary Institute, Houston, TX. Abstract No. 2241.
Laity, J.S., Malin, M.C., 1985. Sapping processes and the development of theater-headed valley networks on the Colorado Plateau. Geol. Soc. Am. Bull. 96 (2), 203–217.
Lamb, M.P., Howard, A.D., Johnson, J., Whipple, K.X., Dietrich, W.E., Perron, J.T., 2006. Can springs cut canyons into rock? J. Geophys. Res. 111, E07002. doi:10.1029/2005JE002663.
Lamb, M.P., Howard, A.D., Dietrich, W.E., Perron, J.T., 2007. Formation of amphitheater-headed valleys by waterfall erosion after large-scale slumping on Hawai'i. Geol. Soc. Am. Bull. 119 (7), 805–822. doi:10.1130/B25986.1.
Lamb, M.P., Dietrich, W.E., Aciego, S.M., DePaolo, D.J., Manga, M., 2008. Formation of Box Canyon, Idaho, by megaflood: Implications for seepage erosion on Earth and Mars. Science 320, 1067–1070. doi:10.1126/science.1156630.
Lyon, R.J.P., 1965. Analysis of rocks by spectral infrared emission (8 to 25 microns). Econ. Geol. 60, 705–736.
Machette, Michael N., Slate, Janet L., Phillips, Fred M., 2008. Terrestrial Cosmogenic-Nuclide Dating of Alluvial Fans in Death Valley, California: U.S. Geological Survey Professional Paper 1755, 45 p.
Malin, M.C. et al., 2007. Context Camera Investigation on board the Mars Reconnaissance Orbiter. J. Geophys. Res. 112. E05S04. doi:10.1029/2006JE002808.
Mars Channel Working Group, 1983. Channels and valleys on Mars. Geol. Soc. Am. Bull. 94 (9), 1035–1054.
McEwen, A.S., Preblich, B.S., Turtle, E.P., Artemieva, N.A., Golombek, M.P., Hurst, M., Kirk, R.L., Burr, D.M., Christensen, P.R., 2005. The rayed crater Zunil and interpretations of small impact craters on Mars. Icarus 176, 351–381. doi:10.1016/j.icarus.2005.02.009.
McEwen, A.S. et al., 2007. Mars Reconnaissance Orbiter's High Resolution Imaging Science Experiment (HiRISE). J. Geophys. Res. 112. E05S02. doi:10.1029/10.1029/2005JE002605.
McGuire, P.C. et al., 2009. An improvement to the volcano-scan algorithm for atmospheric correction of CRISM and OMEGA spectral data. Planet. Space Sci. 57, 809–815. doi:10.1016/j.pss.2009.03.007.
Michalski, J.R., Kraft, M.D., Sharp, T.G., Williams, L.B., Christensen, P.R., 2005. Mineralogical constraints on the high-silica martian surface component observed by TES. Icarus 174, 161–177. doi:10.1016/j.icarus.2004.10.022.
Moore, J.M., Howard, A.D., 2005. Large alluvial fans on Mars. J. Geophys. Res. 110. E04005. doi:10.1029/2004JE002352.
Morris, R.V., Graff, T.G., Mertzman, S.A., Lane, M.D., Christensen, P.R., 2003. Palagonitic (not andesitic) Mars: Evidence from thermal emission and VNIR spectra of palagonitic alteration rinds on basaltic rock. In: Sixth International Conference on Mars, p. 3211.
Murchie, S. et al., 2007. Compact Reconnaissance Imaging Spectrometer for Mars (CRISM) on Mars Reconnaissance Orbiter (MRO). J. Geophys. Res. 112. E05S03. doi:10.1029/2006JE002682.
Neukum, G., Jaumann, R., HRSC Co-Investigator and Experiment Team, 2004. HRSC: The High Resolution Stereo Camera of Mars Express. In: Wilson, A. (Ed.), Mars Express: The Scientific Payload. ESA, Noordwijk, The Netherlands, pp. 17–35.
Pelkey, S.M. et al., 2007. CRISM multispectral summary products: Parameterizing mineral diversity on Mars from reflectance. J. Geophys. Res. 112. E08S14. doi:10.1029/2006JE002831.
Phillips, R.J. et al., 2001. Ancient geodynamics and global-scale hydrology on Mars. Science 291, 2587–2591. doi:10.1126/science.1058701.
Piqueux, S., Christensen, P.R., 2009a. A model of thermal conductivity for planetary soils: 1. Theory for unconsolidated soils. J. Geophys. Res. 114. E09005. doi:10.1029/2008JE003308.
Piqueux, S., Christensen, P.R., 2009b. A model of thermal conductivity for planetary soils: 2. Theory for cemented soils. J. Geophys. Res. 114, E09006. doi:10.1029/2008JE003309.
Poulet, F., Gomez, C., Bibring, J.P., Langevin, Y., Gondet, B., Pinet, P., Bellucci, G., Mustard, J., 2007. Martian surface mineralogy from Observatoire pour la Mineralogie, l'Eau, les Glaces et l'Activite on board the Mars Express spacecraft (OMEGA). J. Geophys. Res. 112. E08S02. doi:10.1029/2006JE002840.
Presley, M.A., Craddock, R.A., 2006. Thermal conductivity measurements of particulate materials: 3. Natural samples and mixtures of particle sizes. J. Geophys. Res. 111. E09013. doi:10.1029/2006JE002706.
Presley, M.A., Craddock, R.A., Zolotova, N., 2009. The effect of salt crust on the thermal conductivity of one sample of fluvial particulate materials under martian atmospheric pressures. J. Geophys. Res. 114. E11007. doi:10.1029/2009JE003355.
Putzig, N.E., Mellon, M.T., 2007. Apparent thermal inertia and the surface heterogeneity of Mars. Icarus 191, 68–94. doi:10.1016/j.icarus.2007.05.013.
Rogers, A.D., Christensen, P.R., 2007. Surface mineralogy of martian low-albedo regions from MGS-TES data: Implications for upper crustal evolution and surface alteration. J. Geophys. Res. 112. E01003. doi:10.1029/2006JE002727.
Ruff, S.W., Christensen, P.R., 2002. Bright and dark regions on Mars: Particle size and mineralogical characteristics based on Thermal Emission Spectrometer data. J. Geophys. Res. 107 (E12). doi:10.1029/2001JE001580.
Ruff, S.W., Christensen, P.R., 2007. Basaltic andesite, altered basalt, and a TES-based search for smectite clay minerals on Mars. Geophys. Res. Lett. 34. L10204. doi:10.1029/2007GL029602.
Schumm, S.A., Boyd, K.F., Wolff, C.G., Spitz, W.J., 1995. A ground-water sapping landscape in the Florida Panhandle. Geomorphology 12, 281–297.
Segura, T.L., Toon, O.B., Colaprete, A., Zahnle, K., 2002. Environmental effects of large impacts on Mars. Science. 298, 1977–1980.
Shoemaker, E.M., 1987. Meteor Crater, Arizona. In: Beus, S.S. (Ed.), Geological Society of America Centennial Field Guide – Rocky Mountain Section. Geological Society of America, pp. 399–404.
Smith, M.D., Bandfield, J.L., Christensen, P.R., 2000. Separation of atmospheric and surface spectral features in Mars Global Surveyor Thermal Emission Spectrometer (TES) spectra. J. Geophys. Res. 105, 9589–9607.
Tanaka, K.L., 1986. The stratigraphy of Mars. J. Geophys. Res. 91 (B13), E139–E158.
Toon, O.B., Segura, T.L., Zahnle, K., 2010. The formation of martian river valleys by impacts. Annu. Rev. Earth Pl. Sc. 38, 303–322.
Williams, R.M.E., Malin, M.C., 2008. Sub-kilometer fans in Mojave Crater, Mars. Icarus 198, 365–383. doi:10.1016/j.icarus.2008.07.013.